This is the peer-reviewed, final accepted version for American Mineralogist, published by the Mineralogical Society of America.
The published version is subject to change. Cite as Authors (Year) Title. American Mineralogist, in press.
DOI: https://doi.org/10.2138/am-2023-8981. http://www.minsocam.org/

Revision 1

Effect of chlorine substitution on the thermal stability of ferro-pargasite and thermochemical properties of ferro-chloro-hornblende

David M. Jenkins[1]

[1] Department of Earth Sciences

Binghamton University

Binghamton, NY 13902

Running title: Chlorine-rich amphibole stability

Abstract

Substitution of chlorine for hydroxyls in calcium amphiboles has been widely documented but the effect of this substitution on thermal stability is not known. Experimental reversal data are presented here comparing the upper-thermal stability of amphiboles formed in the ferro-pargasite and ferro-chloro-pargasite bulk compositions. Experiments were made over the range of 550 – 900°C and 0.5 – 3 kbar at oxygen fugacities of $\log(fO_2)$ of -0.3 to +0.5 relative to Co-CoO. Electron microprobe analysis of amphiboles made from the ferro-pargasite bulk composition were found to be ferro-pargasite, while those made from the ferro-chloro-pargasite

This is the peer-reviewed, final accepted version for American Mineralogist, published by the Mineralogical Society of America.
The published version is subject to change. Cite as Authors (Year) Title. American Mineralogist, in press.
DOI: https://doi.org/10.2138/am-2023-8981. http://www.minsocam.org/

bulk composition were low in A-site Na and Cl and were better classified as Cl-bearing ferro-ferri-hornblende. Although the differences between desired and observed amphibole compositions complicate the comparison of their thermal stabilities, it can be deduced that the Cl-bearing amphibole has a steeper dP/dT slope and, above 1 kbar, a lower thermal stability than ferro-pargasite. Thermodynamic analysis of the Cl-bearing amphibole was also done to extract thermochemical data for the Cl end-member amphibole ferro-chloro-hornblende ($Ca_2(Fe_4Al)(AlSi_7)O_{22}Cl_2$ = Fe-Cl-Horn) that are consistent with the thermodynamic database of Holland and Powell (2011). Using an ideal-activity expression and estimated values for the heat capacity (C_P = 1.106 + 8.9156 X 10^{-5}(T, K) – 11,218.3/T^2 – 5.9548/$T^{0.5}$; kJ/K·mol) and volume (283.0 ± 1.5 cm^3/mole) for Fe-Cl-Horn, the derived values for $\Delta H_f°$ and $S°$ are -10,842.6 ± 10.3 kJ/mol and 618.8 ± 11.1 J/K·mol, respectively. The implication of this work is that (a) chlorine appears to lower the thermal stability of a given calcium amphibole in contrast to the marked increase in thermal stabilities caused by fluorine, and (b) thermochemical data such as those derived in this study allow absolute concentrations of chloride salts to be calculated in metasomatic paleobrines, as illustrated for the Bamble sector of southern Norway reported in the literature.

Keywords: mineral stability, ferro-pargasite, ferro-chloro-hornblende, chlorine amphibole, thermochemistry, metasomatic paleobrines, mineral synthesis

Introduction

Chlorine substitution into calcium amphiboles is well documented throughout a variety of geological settings, such as in oceanic crust (Vanko, 1986; Kendrick et al., 2015, 2022),

metamorphic shear zones (Kullerud, 1996; Johnson et al., 2004), metamorphosed iron formations (Henry and Daigle, 2018), geothermal systems (Enami et al., 1992; Marks et al. 2010), and even Martian meteorites (Giesting and Filiberto., 2016; Martínez et al., 2023). What is largely unknown is the effect that chlorine has on the upper-thermal stability of calcium amphiboles. This stands in contrast to a relatively rich history of experimental studies on F-bearing amphibole synthesis and stability (e.g., Bowen and Schairer, 1935; Comeforo and Kohn, 1954; Holloway and Ford, 1975; Gilbert et al., 1982; Graham and Navrotsky, 1986; Robert et al., 1989; Raudsepp et al., 1991; Jenkins and Hawthorne, 1995; Pavlovich and Jenkins, 2003). With a growing interest in the use of halogens to monitor geological processes ranging from seawater–ocean-crust interactions (e.g., Barnes and Cisneros, 2012; Kendrick et al., 2022) and crustal shear-zone metasomatism (Kusebauch et al., 2015) to mantle metasomatism (Frezzotti et al., 2010; Selverstone and Sharp, 2011) and the formation of economic deposits (Yardley and Bodnar, 2014), there is a need to understand how the incorporation of Cl into calcium amphiboles might affect their stability, particularly relative to the OH-equivalent amphibole. This information would be of interest in understanding the depth to which Cl could be transported in, for example, the mafic portion of subducting lithosphere. It would also be of considerable interest in understanding whether Cl substitution for OH in amphibole might stabilize the amphibole to sufficiently high temperatures to allow Cl-rich amphibole to be stable at solidus temperatures and, therefore, form directly from a silicate melt, as occurs when F substitutes for OH in phlogopite (e.g., Sun et al., 2022).

Essentially all amphiboles that have been documented with significant Cl contents are calcium amphiboles. Giesting and Filliberto (2016) did a thorough literature review of terrestrial and Martian meteorites and found the most common Cl-rich amphiboles to be ferro-pargasite

67 $[(NaCa_2(Fe_4Al)(Al_2Si_6)O_{22}(OH,Cl)_2]$ and potassic-hastingsite
68 $[(KCa_2(Fe_4Fe^{3+})(Al_2Si_6)O_{22}(OH,Cl)_2]$, with less common reports of ferro-edenite
69 $[(NaCa_2Fe_5(AlSi_7)O_{22}(OH,Cl)_2]$, ferro-hornblende [$Ca_2(Fe_4Al)(AlSi_7)O_{22}(OH,Cl)_2]$, and ferro-
70 ferri-sadanagaite $[(NaCa_2(Fe_3Fe^{3+}{}_2(Al_3Si_5)O_{22}(OH,Cl)_2]$, where Fe in the formula is assumed to
71 be Fe^{2+} unless indicated otherwise, and the symbol represents a vacancy on the *A*
72 crystallographic site. The most Cl-rich amphiboles on Earth and in Martian meteorites tend to be
73 potassium-rich, specifically potassic-chloro-hastingsite, having Cl contents up to 1.8 Cl atoms
74 per formula unit (apfu) (Giesting and Filiberto, 2016; Carpenter et al., 2021). This study focuses
75 on pargasitic amphiboles because they are one of the most common amphiboles in metamorphic
76 and igneous rocks, as summarized in the reviews presented by Robinson et al. (1982) and Martin
77 (2007), respectively. Many studies have shown that there is a strong correlation between iron
78 content, often expressed as the iron number ($Fe\# = Fe^{2+}/(Fe^{2+} + Mg)$), and Cl content in calcium
79 amphiboles. This is also referred to as Mg-Cl avoidance as discussed, for example, by Morrison
80 (1991), Kullerud (1996), and Iveson et al. (2017). It is more likely, therefore, that Mg-free ferro-
81 pargasite ($NaCa_2(Fe_4Al)(Al_2Si_6)O_{22}(OH)_2$) would be expected to maximize the Cl content. This
82 in turn should produce the greatest shift in the location of the amphibole stability boundary
83 attributable to incorporation of Cl into its structure. Earlier work done by Chan et al. (2016) and
84 Campanaro and Jenkins (2017) on pargasitic amphiboles showed that Cl strongly partitioned into
85 NaCl brines and would only enter amphibole at any significant level (>0.1 Cl apfu) if the brine
86 was at saturation (~83 wt% NaCl at 700 °C and 2 kb, Driesner and Heinrich, 2007). The use of
87 $FeCl_2$ was found to give somewhat better results (Chan et al., 2016), which was attributed by
88 Jenkins (2019) to the higher Cl activity in this 1:2 salt, but, again, it was the highest $FeCl_2$ brine
89 concentrations that gave the highest amphibole Cl contents (Jenkins, 2019).

In view of the previous research on amphibole formation in various brines, this study examines the upper-thermal stability of Cl-bearing amphibole formed from the bulk composition ferro-chloro-pargasite ($NaCa_2(Fe_4Al)(Al_2Si_6)O_{22}(Cl)_2$) in the range of 0.5 – 3 kbar and compares it to the stability of synthetic OH-bearing ferro-pargasite, all done under hydrogen fugacities (fH_2) corresponding to oxygen fugacities (fO_2) at + 0.5 log(fO_2) above the Co-CoO oxygen buffer or approximately 0.2 log(fO_2) below the fayalite-magnetite-quartz (FMQ) buffer. Chlorine-bearing amphiboles were made in this study using undiluted $FeCl_2$ in nominally "dry" syntheses in order to maximize the Cl content in the amphiboles, though even under these conditions it was difficult to avoid absorption of moisture as discussed below. This work also allows thermochemical values of a chlorine end-member amphibole, namely ferro-chloro-hornblende ($Ca_2(Fe_4Al)(AlSi_7)O_{22}Cl_2$), to be derived. Such information is needed for making quantitative calculations of basic hydrothermal processes including the exchange of Cl between a brine and calcium amphibole.

Methods

Starting materials

All syntheses were made using mixtures of reagent-grade oxides, carbonates, metallic iron, and "$FeCl_2$". The reagents were SiO_2, which was made by desiccating silicic acid by step-wise heating to 1100 °C overnight, Al_2O_3, Fe_2O_3, $CaCO_3$, Na_2CO_3, and metallic Fe (~10 μm grain size). As discussed in Jenkins (2019), the reagent "$FeCl_2$" as received is partially hydrated to $FeCl_2 \cdot 2H_2O$, but could be dehydrated to $FeCl_2$ by heating in air at 160°C for 15 minutes (and still avoiding oxidation to hematite) prior to being sealed in the sample capsule.

Starting mixtures were prepared by first mixing the stoichiometric proportions of SiO_2, Al_2O_3, $CaCO_3$, and Na_2CO_3, together under acetone until dry. This mixture was then heated in

air at 900°C for 15 min to decarbonate the mixture by reaction with SiO_2 but purposely kept to a short duration to minimize volatilization of Na. To this decarbonated mixture was added Fe_2O_3 and metallic Fe in proportions equivalent to the required FeO, along with "$FeCl_2$", adjusted for the proportion of iron chloride di-hydrate present (from XRD analysis). Two bulk compositions were investigated in this study, namely ferro-chloro-pargasite, with the bulk composition $NaCa_2(Fe_4Al)(Al_2Si_6)O_{22}(Cl_2)$ (sample code prefix of FEPG 1), and ferro-pargasite, expressed here as it was prepared in its anhydrous form $NaCa_2(Fe_4Al)(Al_2Si_6)O_{23}$ (sample code prefix of FEPG 3). The Fe is ferrous iron in both formulae.

Sample treatment

Portions of the starting materials were encapsulated in $Ag_{50}Pd_{50}$ alloy capsules made from tubing that was either 3.0 mm outer diameter (OD), for synthesis experiments, or 1.5 mm OD, for reaction reversal experiments, both having 0.13 mm wall thicknesses. Mixtures containing "$FeCl_2$" were heated at 160°C for 15 min in air, crimped while still hot (to minimize subsequent exposure to air), and then sealed dry by arc welding under a lightly moistened tissue to help mask the AgPd-melt from exposure to oxygen (Weidner, 1989). Experiments on ferro-pargasite (without Cl) were done in the presence of about 7 wt% H_2O.

Apparatus

The majority of the experiments in this study were done with internally-heated gas vessels. Specific mixtures of hydrogen and argon were used to impose a reducing atmosphere. This gas mixture was made by first charging the vessel and the gas intensifier with a predetermined pressure of hydrogen, typically in the range of 1.4 – 14 bars. Once at a given hydrogen pressure, the system was then pumped with argon to achieve a desired total pressure of H_2-Ar, typically in the range of 400-1000 bars, from which the mole fraction of H_2 could be determined. The

hydrogen fugacity was calculated at the final pressure and temperature (*P*-*T*) conditions of the experiment by multiplying the fugacity coefficient for H_2 (γ_{H2}, Shaw and Wones, 1964) at the corresponding *P*-*T* conditions by the mole fraction of H_2 in the gas, i.e., $f_{H2} = P \cdot X_{H2} \cdot \gamma_{H2}$. One can calculate the oxygen fugacity (fO_2) resulting from imposing a known hydrogen fugacity on a given water fugacity knowing the equilibrium constant for the reaction $H_2O = H_2 + 0.5\ O_2$ at the *P*-*T* conditions of interest. This method was confirmed using Co-CoO-MnO oxygen sensor calibration experiments as discussed in Jenkins (2019). It should be noted that the experiments on the ferro-chloro-pargasite bulk composition were done essentially dry, with any water present being only the moisture absorbed by the reagents (particularly "$FeCl_2$") during capsule welding. For these experiments, the reported fO_2 is provided simply for the sake of comparison with equivalent water-bearing experiments both in this study and others in the literature.

Two syntheses (FEPG 1-11, FEPG 1-14) were done in externally-heated cold-seal vessels made of the Ni-rich alloy René 41. These experiments were done using water as the pressure medium but included a short length of iron rod to act as an oxygen getter to draw down the oxygen fugacity below that of the normal Ni-NiO conditions for these vessels. Assessment of the approximate oxygen fugacity achieved using this method as indicated in Table 1 is discussed in Chan et al. (2016) and Jenkins (2019).

Analytical methods

Powder X-ray diffraction (XRD) patterns were obtained on a Panalytical PW3040-MPD X-ray diffractometer operated at 40 kV and 20 mA using Cu K_α radiation with a graphite diffracted-beam monochromator. Samples were mounted on a zero-background quartz plate, scanned using a step size of 0.04° 2Θ, and measured for durations sufficient for obtaining 600 –

158 1000 counts on the strongest peaks. Rietveld refinements were made using the General Structure
159 Analysis System – II (GSAS-II) software of Toby and Von Dreele (2013).

160 Electron microprobe analysis was done on a JEOL 8900 Superprobe using samples mounted
161 in epoxy and polished with diamond abrasive in successively finer grits to a final size of 0.5 μm.
162 The operating conditions for all analyses were 15 kV and 10 nA using albite as the standard for
163 Na, wollastonite for Ca, the pure oxides for Fe, Al, and Si, orthoclase for K, and reagent $PdCl_2$
164 for Cl. Matrix corrections were made with the ZAF scheme. The electron beam size was used in
165 spot mode (~1 μm diameter) because of the small grain sizes of the synthetic amphiboles (~3 x 6
166 μm in plan view). Counting times for WDS analyses of the major elements (Na, Al, Si, Ca, and
167 Fe) were kept to 10 s on the peak and 3 s on the background to minimize Na diffusion from the
168 standards and possibly from the samples. Because of the relatively low Cl contents observed for
169 many of the amphiboles, Cl was measured using 30 s on the peak and 10 s on the background. It
170 should be noted that analysis of fine-grained minerals, such as the amphiboles formed in this
171 study, often results in the X-ray excitation volume exceeding the volume of the grain and
172 resulting in low analytical totals. This situation has been studied in considerable detail in this lab
173 (e.g., Giblin et al., 1993; Jenkins and Corona, 2006) where it has been shown that analyses with
174 analytical totals even as low as 65-70 wt% give stoichiometries that are essentially equivalent to
175 coarse-grained minerals. In this study, most analyses were well above this minimum, typically
176 in the range of 80-98 wt%.

177 Cations were calculated from the oxide and Cl weight% as follows. Plagioclase was
178 calculated on the basis of 8 oxygens and assuming any iron present has a ferric-iron fraction (=
179 $Fe^{3+}/(Fe^{2+} + Fe^{3+})$) of 0.7, which is the approximate average value found for gabbroic plagioclase
180 by Nakada et al. (2019). Pyroxene was calculated on the basis of 6 oxygens with all iron

assumed to be Fe^{2+}. Amphibole, with the general formula of $AB_2C_5T_8O_{22}W_2$, was calculated initially assuming all iron was ferrous and adding sufficient OH to have the sum of OH+Cl in the W sites equal 2.0. In many cases this did not result in a feasible amphibole formula (e.g., cation sums above 16.0, deficient C-site cations, etc.), in which case ferric iron was introduced under the assumption that the ferric-iron proportion (= $Fe^{3+}/\sum Fe$) was a constant value of 18%. This value is based on the studies of Chan et al. (2016) and Mueller et al. (2017) where amphiboles were synthesized from the bulk compositions of ferro-pargasite and along the magnesio-hastingsite–hastingsite [$NaCa_2(Mg_4Fe^{3+})(Al_2Si_6)O_{22}(OH)_2$- $NaCa_2(Fe_4Fe^{3+})(Al_2Si_6)O_{22}(OH)_2$] join, respectively, using the same experimental methods and techniques used in this study. Further discussion for the choice of 18% ferric iron can be found in Campanaro and Jenkins (2017). Cations for ferric-oxide-corrected microprobe analyses were then determined by having the sum of O+OH+Cl = 24 and either adding sufficient OH to have the sum of OH+Cl in the W sites equal 2.0, or sufficient OH to have the sum of T- and C-site cations (excluding Ca, Na, and K) equal 13. The former method of adding OH to have the sum of OH + Cl be 2.0 can cause a surplus of positive charges and a resultant deficiency of C-site cations to maintain charge balance. The latter method allows for a deficit of OH and therefore the presence of oxo-amphibole component, something that has been well documented for Ti-bearing pargasite and kaersutitic amphiboles by Popp and Bryndzia (1992). Cations were distributed in a conventional manner, namely filling the T sites first with Si then Al to sum to 8, assigning the remaining Al, Fe^{3+}, and sufficient Fe^{2+} (in that order) to the C sites to sum to 5, putting excess Fe^{2+} into the B sites along with sufficient Ca and Na to sum to 2, and assigning any remaining Ca, Na, and K to the A sites. This method also minimizes the A-site Ca content which, though feasible for calcium amphiboles, is generally found only for Ti-rich amphiboles (e.g., kaersutite, Hawthorne

et al., 2012). Resultant mineral formulae with cation totals below 15.0 or above 16.05 were rejected.

Infrared spectra were obtained for several samples using a Bruker Tensor 27 FTIR instrument, acquired in a nitrogen-purged chamber as the average of 64 scans at a resolution of 2 cm^{-1}. About 7-8 mg of sample was mixed with 200 mg KBr and pressed into a 13 mm disc in an evacuable pellet die.

Results

Ferro-chloro-pargasite bulk composition

Conditions used to make the starting materials for the ferro-chloro-pargasite experiments and the synthesis products are listed in Table 1. Representative back-scattered-electron (BSE) images of the amphibole-growth and breakdown materials are shown in Figures 1a and 1b, respectively. Generally, the amphibole and clinopyroxene have a similar grey-level brightness but are usually distinguished from each other by amphibole having the more fibrous or elongate habit while pyroxene has a more equant habit and is often larger. All of the other phases are readily identified by their different BSE grey levels. Chemical analyses of amphibole and its breakdown products are given in Table 2. Despite having the bulk composition of ferro-chloro-pargasite, the amphiboles that were formed are actually ferro-ferri-hornblende, if adhering to the ferric-iron fraction of 0.18. If the ferric-iron fraction is varied to satisfy the conditions that (a) the sum of cations excluding Ca and Na must sum to 13 and (b) the sum of OH + Cl = 2.00, then the ferric-iron fraction is higher moving the amphibole into the field of ferro-ferri-tschermakite (Locock, 2014). In either case, the Na content at the A site is distinctly low; Na that is excluded from the amphibole goes in to forming halite, a phase that was *not* used as part of the reagents in the starting mixture. The presence of halite also indicates that there is ample Na available (at

227 saturation) and that the low Na content is a crystal chemical restriction at these pressure-
228 temperature-composition conditions of formation.

229 Starting mixtures for the reaction-reversal experiments relevant to the ferro-chloro-pargasite
230 bulk composition (CLFP-1, -2) are listed in Table 3, while results for the reversal experiments
231 are given in the upper portions of Table 4. Chemical analyses of amphiboles, pyroxenes, and
232 plagioclase from selected reaction-reversal experiments are listed in Tables 5, 6, and 7,
233 respectively. Preliminary experiments were done at an oxygen fugacity of 0.3 log(fO_2) units
234 below the Co-CoO buffer in order to minimize the ferric-iron content of the amphibole and
235 maximize the ferro-pargasite component. These experimental results are listed in the top portion
236 of Table 4 as having been done at a "lower fO_2". Unfortunately, the high hydrogen partial
237 pressures needed to maintain this low oxygen fugacity had the detrimental effect of leading to
238 gas vessel failure from hydrogen embrittlement (e.g., Fletcher and Elsea, 1964). Therefore, most
239 of the experiments were done at an oxygen fugacity 0.5 log(fO_2) above Co-CoO, which is about
240 0.1 to 0.3 log(fO_2) units below the fayalite-magnetite-quartz buffer, depending on the
241 temperature. These results are listed in Table 4 as having been done under "higher fO_2"
242 conditions.

243 Sufficient experiments were done at the lower fO_2 to provide some idea of the sensitivity of
244 the thermal stability of Cl-bearing amphibole to the oxygen fugacity. Figure 2 shows the results
245 for the ferro-chloro-pargasite bulk composition at the higher (circles) and lower (triangles)
246 oxygen fugacities. The solid line is a linear regression to the bracketing experimental data at the
247 higher fO_2 while the dashed line is an estimate fit by eye to the lower fO_2 data. At 1 kbar the two
248 sets of data overlap within the accuracy of the data. At higher pressures the limited number of
249 data points do not offer very clear constraints on the location of the boundary; however,

amphibole breaks down at a slightly lower temperature (~10°C) at 2 kbar and 640°C and shows no reaction at 600°C and 1.75 kbar suggesting the breakdown boundary lies at 620 ± 20°C. Overall, a reduction of 0.8 in $\log(fO_2)$ amounts to a decrease in the amphibole breakdown boundary of 15-30°C in the range of 1-2 kbar. This is opposite to what was observed by Gilbert (1966) for ferro-pargasite, where there was an approximately 105°C *increase* in thermal stability in going from a higher fO_2 (Ni-NiO) to about 0.7 $\log(fO_2)$ lower values (fayalite-magnetite-quartz). It should be stressed that the experiments done on the ferro-chloro-pargasite bulk composition were done with no added water, which means that the oxygen fugacities are likely lower than the corresponding water-rich assemblage (Matjuschkin et al., 2015). The oxygen fugacities reported here are, therefore, considered maximum values.

Chemical analyses were obtained for two amphiboles (CLFP 1-6, CLFP 2-7) treated at nearly the same temperature (630-640°C) and pressure (2 kbar) but under these two different oxygen fugacities to see what, if any, effect this has on the amphibole composition. Experiment CLFP 1-6 was run at the lower fO_2 and, though showing a net breakdown in amphibole, had sufficient amphibole present (~30 wt%) to acquire adequate analyses. Comparing the chemical analysis of this sample with CLFP 2-7, run at the higher fO_2, in Table 5, one can see that their compositions are very similar, having only minor differences (≤0.16 apfu) on any site. If the cations are calculated without imposing a fixed ferric-iron fraction but instead allowing them to vary so as to have 13 cations excluding Ca and Na and the sum of OH + Cl be 2, then CLFP 1-6 $(Na_{0.27}(Ca_{1.68}Na_{0.32})(Fe_{3.60}Fe^{3+}_{1.09}Al_{0.31})(Al_{1.35}Si_{6.65})O_{22}(OH_{1.51}Cl_{0.49}))$ actually has a slightly *higher* ferric-iron content than CLFP 2-7 $(Na_{0.38}(Ca_{1.75}Na_{0.25})(Fe_{3.68}Fe^{3+}_{0.83}Al_{0.49})(Al_{1.44}Si_{6.56})O_{22}(OH_{1.55}Cl_{0.45}))$ even though the former was made at the lower fO_2. Both amphiboles continue to be classified as ferro-ferri-hornblendes

regardless of whether the ferric-iron is fixed or allowed to vary. In summary, there is no significant difference in the compositions of the amphiboles formed at these two different oxygen fugacities, which also accounts for the similarities in their stability boundaries.

Ferro-pargasite bulk composition

The starting materials for the ferro-pargasite experiments are listed in Table 1. Representative back-scattered-electron (BSE) images of the amphibole-growth and breakdown materials are shown in Figures 1c and 1d, respectively. As with the ferro-chloro-pargasite bulk composition, the clinopyroxene and amphibole have similar grey-level brightness but are usually distinguished from each other by their habit. Compositions of the starting amphibole and its breakdown products are given in Table 2, while reversal mixtures used for these experiments are given in Table 3. In contrast to the ferro-chloro-pargasite bulk composition, the amphibole formed from the ferro-pargasite bulk composition (FEPG 3-24) is classified as ferro-pargasite.

Reaction reversal experiments done with the ferro-pargasite bulk composition are listed in the lower portion of Table 4 and shown in Figure 3. Compositions of amphiboles, pyroxenes, and plagioclase from selected reaction-reversal experiments are listed in Tables 5, 6, and 7, respectively. Hercynitic spinel is observed as one of the breakdown products in BSE images, usually as minor inclusions in plagioclase, but is generally not observed in the XRD patterns or only at a level of about 1 wt% (FEPG 3-26). Also shown in Figure 3 is the upper-thermal stability curve of ferro-pargasite reported by Gilbert (1966) determined at the fayalite-magnetite-quartz (FMQ) oxygen buffer. This oxygen fugacity is slightly higher (0.2 $\log(fO_2)$) than what was used in this study. The upper-thermal stability curve shown in Figure 3 is simply a straight-line fit to the data as there are insufficient data to determine what, if any, curvature exists for this dehydration boundary. Although the two studies are in close agreement at 1 kbar, the current study places the boundary approximately 150°C higher than that of Gilbert (1966) at 2 kbar. As

297 discussed below, this boundary is provided primarily as a frame of reference for understanding
298 the effect of Cl on the stability of calcium amphibole at a given oxygen fugacity.

299 **Discussion**

300 **Effect of Cl on the stability of calcium amphibole**

301 Figure 4 shows a comparison of the upper-thermal stability of the ferro-ferri-hornblende (Fig.
302 4a) made in this study from the ferro-chloro-pargasite bulk composition with the upper-thermal
303 stability of chlorine-free ferro-pargasite (Fig. 4b), both treated at the same hydrogen-equivalent
304 oxygen fugacity. The ferro-ferri-hornblende has about 0.45 apfu Cl (Table 5). Direct comparison
305 of their relative stabilities is complicated by the differences in their Si, Al, and particularly Na
306 contents, in addition to the presence or absence of Cl. However, the substitution of Cl for OH in
307 what is otherwise the same bulk composition and treated at the same oxygen fugacity results in
308 an amphibole with lower thermal stability. This stands in striking contrast to F which is well
309 known to cause pronounced increases in the thermal stability of (Mg-rich) amphiboles and micas
310 (e.g., Gilbert et al., 1982; Aranovich and Safonov, 2018; Sun et al., 2022). From this study, Cl
311 appears to reduce the thermal stability of amphibole above 1 kbar, lowering the stability by about
312 150° C at 2 kbar. The steeper slope of the Cl-bearing amphibole boundary in Figure 4a
313 compared to the OH-amphibole in Figure 4b suggests that the Cl-amphibole would be more
314 stable below 1 kbar, but the sluggish kinetics encountered below 1 kbar prevents experimental
315 confirmation of this hypothesis.

316 **Thermodynamic treatment**

317 The experimental results observed here (Fig. 4a) on the upper-thermal stability of the Cl-
318 bearing amphibole ferro-ferri-hornblende provides an opportunity to derive, to at least a first
319 approximation, thermochemical values for an end-member calcium Cl-amphibole. Such
320 information would be extremely useful for the geological community by allowing the chloride

composition of the brine from which the amphibole formed to be determined, so long as the appropriate mineral assemblage was present. Because of the "intermediate" composition of the Cl-OH-amphibole observed in this study, it is possible to derive the thermochemical values for several different end-member Cl-amphiboles with essentially the same degree of uncertainties. Accordingly, the values of the enthalpy of formation (ΔH_f°) and third-law entropy (S°) for ferro-chloro-hornblende ($Ca_2(Fe_4Al)(AlSi_7)O_{22}Cl_2$) will be extracted from the experimental data using a fairly well constrained value for its volume and reasonable estimate for its heat capacity expression. This component was chosen because it only involves five chemical components and therefore makes it more useful for writing chlorine-buffering chemical reactions.

The method used here is the *G'* vs *T* method described in detail in previous publications (e.g., Welch and Pawley, 1991; Almeida and Jenkins, 2017). In brief, this method uses the simplified thermodynamic expression:

$$\Delta G_{P,T} = 0 = \Delta H^o - T\Delta S^o + \mathrm{f}\left(\Delta C_P, \Delta V^{solids}, K_a\right) \quad (1)$$

where $\Delta G_{P,T}$ is the Gibbs free-energy of the reaction at the pressure (P) and temperature (T, in K) of interest and must be zero at equilibrium, while the last term represents a function of the heat capacity change (ΔC_P), volume change of the solids (ΔV^{solids}), and equilibrium constant (K_a) for the reaction. At a given P and T the last term in (1) has a fixed value which is called *G'* and equation (1) can therefore be rearranged to give:

$$-\Delta H^o + T\Delta S^o = G' \quad (2)$$

Plotting *G'* versus *T* defines a straight line whose slope is ΔS° (= $\Delta S_{Reaction}$) and intercept is $-\Delta H^\circ$ ($\Delta H_{Reaction}$) of the reaction at the reference pressure and temperature. From these values, one can derive ΔH_f° and S° for the phase of interest by the expression:

$$\Delta H_f^o = \Sigma\Delta H_f^o(products) - \Delta H_{Reaction} \quad (3)$$

This is the peer-reviewed, final accepted version for American Mineralogist, published by the Mineralogical Society of America.
The published version is subject to change. Cite as Authors (Year) Title. American Mineralogist, in press.
DOI: https://doi.org/10.2138/am-2023-8981. http://www.minsocam.org/

$$S^o = \Sigma S^o(products) - \Delta S_{Reaction} \quad (4)$$

where $\Delta H_f°$(*products*) and *S°(products)* are the sum of the enthalpies of formation and third-law entropies, respectively, of all the other phases multiplied by their corresponding molar coefficients in the reaction of interest.

Considering the phases observed for the breakdown of the Cl-OH-amphibole in Table 4, one reaction that can be written involves the end-member ferro-chloro-hornblende (= Fe-Cl-Horn):

$$\text{Fe-Cl-Horn}^{\text{Amph}} + 2\ \text{CaTs}^{\text{Cpx}} = \text{Fay} + 3\ \text{An}^{\text{Plag}} + \text{Hed}^{\text{Cpx}} + \text{Lawr} \quad (5)$$

where X^Y is component X in phase Y, CaTs is the Ca-tschermak ($CaAl_2SiO_6$) component in clinopyroxene (Cpx), Fay is fayalite (Fe_2SiO_4), An is the anorthite ($CaAl_2Si_2O_8$) component in plagioclase (Plag), Hed is the hedenbergite ($CaFeSi_2O_6$) component in clinopyroxene, and Lawr is lawrencite ($FeCl_2$). Because this reaction involves two components in clinopyroxene it is actually divariant rather than univariant. There is insufficient precision in the experimental data to clearly define the width of the divariant field, but it is expected to be comparable to the experimentally determined temperature range over which complete amphibole breakdown occurs with increasing temperature or loss of a reactant phase with decreasing temperature during amphibole growth (~ 50 °C in this study). This is similar to the multi-variant fields bounding the stability limits of magnesium-rich glaucophane calculated by Corona et al. (2013). Unfortunately, there are insufficient thermodynamic data and calibrated activity-composition relations for iron-rich, let alone chlorine-rich, amphiboles to calculate the width of any multi-variant field in this study. So long as the compositions of the phases are fixed one can at least calculate an isopleth within this divariant field, as will be done here, to provide an initial step in establishing thermochemical data for chlorine-rich calcium amphiboles.

This is the peer-reviewed, final accepted version for American Mineralogist, published by the Mineralogical Society of America.
The published version is subject to change. Cite as Authors (Year) Title. American Mineralogist, in press.
DOI: https://doi.org/10.2138/am-2023-8981. http://www.minsocam.org/

366 Estimates of the volume and heat capacity of end-member ferro-chloro-hornblende were
367 made as follows. Volume was estimated in two ways. The first used the multiple-regression
368 equations determined by Hawthorne and Oberti (2007) based on the OH-rich amphiboles in the
369 database compiled by IGG-CNR Pavia University, Italy, giving a unit-cell volume of 917.3 ± 2.2
370 $Å^3$ (= 276.2 ± 0.7 cm^3/mole) for $Ca_2(Fe_4Al)(AlSi_7)O_{22}(OH)_2$. To accommodate the substitution
371 of Cl for OH, the volume expansion observed in going from OH-apatite to Cl-apatite was
372 applied, where Cl-apatite ($Ca_5(PO_4)_3Cl$) has a very similar Cl content (6.8 wt%) to that of ferro-
373 chloro-hornblende (7.2 wt%). Using the volume data of Hughes et al. (1989) and Hovis et al.
374 (2015) for OH- and Cl-apatite, respectively, the calculated volume of (OH-)ferro-hornblende
375 needs to be increased by 3% to give an estimated volume of 284.5 ± 0.7 cm^3/mole. The second
376 method used the multiple-regression equations formulated by Matteucci (2022) based primarily
377 on the unit-cell dimensions of iron- and chlorine-rich amphiboles synthesized here at
378 Binghamton University; this method allows direct calculation of chlorine end-member
379 amphiboles. For ferro-chloro-hornblende the calculated volume is 281.4 ± 0.5 cm^3/mole. Both
380 of these estimates are reasonably close to the observed volumes for the Cl-OH-amphiboles
381 (ferro-ferri-hornblende) synthesized here, where FEPG 1-11 and FEPG 1-14 have volumes of
382 281.20 ± 0.03 and 280.66 ± 0.06 cm^3/mole, respectively. Averaging the volumes from these two
383 estimation methods gives a volume of 283.0 ± 1.5 cm^3/mole for ferro-chloro-hornblende, which
384 is adopted here. A heat-capacity (C_P) expression for ferro-chloro-hornblende was estimated by a
385 simple summation of monoclinic amphibole and pyroxenes (both being chain silicates) with Cl
386 introduced by subtracting portlandite ($Ca(OH)_2$) and adding hydrophilite ($CaCl_2$) according to
387 the following expression:
388 $$\text{Fe-Cl-Horn} = \text{Fe-Act} + \text{CaTs} - \text{Hed} - Ca(OH)_2 + CaCl_2 \quad (6)$$

where Fe-Act is ferro-actinolite ($Ca_2Fe_5Si_8O_{22}(OH)_2$). Heat capacity expressions for all of the phases on the right side of equation (6) are available in the database of Holland and Powell (2011) except for portlandite and hydrophilite, which were taken from Robie and Hemingway (1995). The resultant C_P expression for ferro-chloro-hornblende is given in Table 8.

The least-well known part of the *G'* term in equation (1) is the equilibrium constant based on activities (K_a). Although the thermochemical activities for the An component in plagioclase and the Hed and CaTs components in clinopyroxene can be readily calculated using the program AX62 (Holland, 2019) which is compatible with the Holland and Powell (2011) database, the activity of the Fe-Cl-Horn component in amphibole and the activity of $FeCl_2$ are more problematic. Without appropriate interaction parameters for the Fe-Cl-rich amphibole component considered here, the simplest approach is to adopt an ideal activity expression similar to that used by Holland and Powell (2011) for amphiboles, with the understanding that this simplistic treatment will be subject to revision as additional data become available in the future. Ideal activity expressions for amphiboles used by Holland and Powell (2011) are basically determined by the configurational entropy arising from cation mixing on each site with the notable exception of the tetrahedral *T*(1) sites, where the mixing of Si and Al is quartered (Dale et al., 2005) in an effort to minimize the very strong effect that the tetrahedral cations exert on the ideal activities. For the *O*(3) (= W) site, it was found by Chan et al. (2016) that thermodynamic consistency in their brine-amphibole exchange experiments was attained when the mole fraction of Cl at the O(3) site was raised to the $(2/3)^{rd}$ power; this is also adopted here because of the chemical similarities between the amphiboles of this study and those studied by Chan et al. (2016). With this revision, the Fe-Cl-Horn component has the ideal activity expression:

This is the peer-reviewed, final accepted version for American Mineralogist, published by the Mineralogical Society of America.
The published version is subject to change. Cite as Authors (Year) Title. American Mineralogist, in press.
DOI: https://doi.org/10.2138/am-2023-8981. http://www.minsocam.org/

412 $$a^{ideal}_{Fe-Cl-Horn} = X^{A}_{\square}(X^{M4}_{Ca})^2(X^{M13}_{Fe2+})^3(2X^{M2}_{Fe2+})(2X^{M2}_{Al})(4X^{T1}_{Al})^{1/4}\left((4/3)X^{T1}_{Al}\right)^{3/4}(X^{O3}_{Cl})^{2/3} \quad (7)$$

413 where X^{j}_{i} is the mole fraction of element *i* on crystallographic site *j*, the symbol represents a
414 vacancy on the *A* crystallographic site, and the constants are needed to ensure that the ideal
415 activity is unity for the pure end member (e.g., Price, 1985). Noting that the amphibole
416 compositions do not vary strongly along the breakdown boundary (Table 5), the average
417 composition of the amphibole observed here, namely
418 $Na_{0.40}(Ca_{1.73}Na_{0.22}Fe_{0.05})(Fe_{3.71}Al_{0.47}Fe^{3+}_{0.82})(Al_{1.39}Si_{6.61})O_{22.08}(Cl_{0.45}OH_{1.47})$, has the
419 corresponding ideal activity of the Fe-Cl-Horn component of 0.0542.

420 The extremely hygroscopic nature of lawrencite makes it difficult to ensure that anhydrous
421 $FeCl_2$ is present in the starting mixture, even when heated to 160 °C just prior to crimping the
422 capsule shut for arc welding. Aside from the OH needed to achieve a feasible amphibole
423 stoichiometry listed in Tables 2 and 5, there are two other lines of evidence to indicate that water
424 is present in these experiments. First, OH-stretching bands are observed in the FTIR spectra for
425 the Cl-OH-amphiboles made here (FEPG 1-11, FEPG 1-14), even though they were made under
426 nominally anhydrous conditions. Figure 5 shows the infrared spectra of the Cl-OH-amphiboles
427 in the OH-stretching region and compares them to the spectrum of the OH-amphibole (FEPG 3-
428 24). Although a detailed assignment of these bands is beyond the scope of this study,
429 preliminary band assignments, based on the extensive data already published for monoclinic
430 amphiboles (Hawthorne and Della Ventura, 2007), suggest that the band at 3657 cm^{-1} is assigned
431 to OH with a local configuration of Fe-Fe-Fe-SiAl-Na, while the band at 3606 cm^{-1} is assigned
432 the configuration Fe-Fe-Fe-SiAl- , with all iron being Fe^{2+}. For the OH-amphibole (FEPG 3-24,
433 ferro-pargasite), the relatively strong band at 3657 cm^{-1} and weak band at 3606 cm^{-1} agrees with
434 the relatively high proportion (84%) of Na and low proportion (16%) of vacancy ( ),

435 respectively, on the *A* site. The opposite is the case for the Cl-OH-amphiboles (FEPG 1-11, 1-
436 14, ferro-ferri-hornblende) where the *A* site is dominated (~70%) by vacancies, giving a
437 correspondingly stronger band at 3606 cm^{-1}. The broad band in the range of 3200-3500 cm^{-1} is
438 attributed to moisture absorbed by the sample, which is often observed for synthetic amphiboles
439 (e.g., Della Ventura et al., 2019) and which appears despite rinsing any salts out of the sample,
440 preparing the KBr pellet under vacuum, and keeping the pellet at 110°C just prior to
441 measurement. Regardless of their exact assignments, the distinct bands identified in Figure 5 can
442 be attributed to OH-stretching in the amphibole structure and indicate that H_2O was present at
443 the time they formed. Second, capsules were routinely weighed after each treatment to ensure
444 the capsule seal held, after which they were pierced with a small cut, dried at 110 °C for periods
445 of 15 min to an hour, and weighed again. There was usually an observable weight loss
446 amounting to about 3 wt% of the sample, which is attributed to water. In view of this evidence,
447 there is at least some water present during the "dry" reversal experiments suggesting that the
448 lawrencite was probably part of a brine rather than only solid $FeCl_2$ and that amphibole is always
449 being formed in a concentrated brine. The exact concentration is simply not known, though
450 using the cut-and-dry assessment of water content and maximum amount of $FeCl_2$ present in the
451 starting mixture gives a mole fraction of $FeCl_2$ (X_{FeCl2}) of about 0.30 ± 0.04. Assuming the
452 solubility of $FeCl_2$ at elevated pressures and temperatures is similar to that of NaCl (Driesner and
453 Heinrich, 2007), this concentration is expected to be below saturation in $FeCl_2$. In view of this
454 uncertainty, thermodynamic data will be derived for a range of mole fractions (assumed equal to
455 activities) of $FeCl_2$ in the brine.

456 Shown in Figure 6 is the G' vs T plot for the case where X_{FeCl2} is 0.30, with the derived
457 values of $\Delta H_f°$ and $S°$ for ferro-chloro-hornblende listed in Table 9. Also given in Table 9 are

This is the peer-reviewed, final accepted version for American Mineralogist, published by the Mineralogical Society of America.
The published version is subject to change. Cite as Authors (Year) Title. American Mineralogist, in press.
DOI: https://doi.org/10.2138/am-2023-8981. http://www.minsocam.org/

458 the values of ΔH_f° and S° derived from the same reaction boundary but assuming the X_{FeCl2} is 0.1
459 and 0.5, the likely limits to the $FeCl_2$ concentration at pressure and temperature. It is noted that
460 only the slope, not the intercept, varies because K_a is only a function of temperature in this
461 analysis, with the result being that only the derived entropy changes. Thermochemical values for
462 the case where X_{FeCl2} is 0.30 are the preferred values.

463 **Geological controls on Cl content in amphibole**

464 There are now sufficient experimental data to allow at least some of the hypotheses
465 concerning geological controls on Cl incorporation into calcium amphiboles to be tested. First,
466 the studies of Campanaro and Jenkins (2017) and Mueller et al. (2017) have confirmed a positive
467 correlation between Cl content and the Fe#, a correlation that is widely observed for both
468 amphiboles and biotites (e.g., Henry and Daigle, 2018). It is for this reason the present study
469 dealt with Mg-free amphibole with Fe# of 1.0 in order to maximize its Cl content. Second, the
470 positive correlations of *A*-site cations (K in particular) and tetrahedral Al with Cl are quite clear
471 from natural amphiboles but have not been fully confirmed experimentally. Jenkins (2019)
472 showed a positive correlation between K and Cl content for hastingsite with Fe# of 1.0 made
473 with concentrated $FeCl_2$ brines for which Na was gradually replaced by K; however, Matteucci
474 et al. (2022) also investigated the formation of hastingsite with Fe# of 1.0 but used a wide range
475 of brine compositions and found that the brine concentration, not the K# (= K/(Ka+Na)), exerted
476 the main control on the Cl content. Extant experimental studies have not been able to adequately
477 test the effect of ^{IV}Al on Cl, as discussed in Jenkins (2019), because the strong correlation of ^{IV}Al
478 with Na and K makes it difficult to test the influence of ^{IV}Al independently of the *A* site
479 occupancy. Third, the role of pressure and temperature have been investigated, where Jenkins
480 (2019) investigated the former and found that the Cl content showed no dependence on pressure

in the range of 2 – 4.5 kbar, while the latter was investigated in this study where the presence of Cl was found to reduce the thermal stability of pargasitic amphibole relative to the OH end-member. Lastly, the effect of oxygen fugacity, as indicated by the ferric iron content, appears to have a complex correlation with Cl content. Mueller et al. (2017) made hastingsitic amphiboles with a range of Fe# using "dry" syntheses with $FeCl_2$ (actually concentrated brines) and found the Cl content of the amphibole to decrease with increasing ferric iron. Matteucci et al. (2022), on the other hand, synthesized hastingsitic amphiboles over a wide range of $FeCl_2$ brine concentrations and observed Cl to increase with increasing ferric iron, up to a brine concentration of about 24 molal $FeCl_2$ ($X_{FeCl2} = 0.30$), above which the Cl content was uncorrelated with ferric iron. Additional details on the roles of the *A*-site cation and ferric-iron on Cl content will be presented in a future manuscript.

Implications

The reduction in the thermal stability of ferro-pargasite with the addition of Cl has several implications. First, incorporation of Cl into amphibole at relatively shallow levels, such as at mid-ocean ridges, will eventually lead to a lower thermal stability compared to Cl-free amphibole in subduction zones. For example, amphibole with 0.45 Cl apfu will breakdown 150° C lower at 2 kbar than (OH-)ferro-pargasite. Using a linear thermal gradient of 10°C/km for a "warm subduction" zone (Cloos, 1993) one would predict the Cl-bearing amphibole to break down at least 15 km shallower than ferro-pargasite. Second, lowering of the thermal stability of calcium amphibole by the presence of Cl makes it even less likely that Cl-bearing amphiboles would form directly from a hydrous magma. Ferro-pargasite, unlike (Mg-)pargasite, was not observed by Gilbert (1966) to be stable at solidus conditions; the addition of up to 0.5 Cl apfu acts to further lower its thermal stability. It should be noted that some of the most Cl-rich

amphiboles observed in nature (some reaching 2.0 Cl apfu) are those occurring in Martian meteorites, though always occurring within melt inclusions hosted by cumulus pyroxenes, olivine, or apatite (e.g., Sautter et al., 2006; Giesting and Filiberto, 2016; Martínez et al., 2023), and that these amphiboles are perhaps the best candidates for having formed directly from a melt.

With the thermochemical data for ferro-chloro-hornblende derived in this study, it is possible to determine the concentrations of specific salts present in the paleobrine from which an amphibole formed, so long as the appropriate mineral assemblage and an independent estimate of pressure and temperature are available.

To illustrate the method, concentrations of two salts, namely $FeCl_2$ and $CaCl_2$, will be determined for the paleobrine that gave rise to the Cl-rich amphiboles in the Bamble sector of southern Norway, as reported by Kusebauch et al (2015). The geology of this locality, in brief, consists of middle Proterozoic amphibolite to granulite facies para- and orthogneisses with a strong NE-SW trending structural pattern (Engvik et al., 2011). Extensive metasomatism, associated with shear zones on a scale of 1 – 10 m, occurred during the latter stages of the Sveconorwegian orogeny (1090-1040 Ma) and converted olivine gabbros to scapolitized metagabbros. A detailed study of the mineralogical and chemical changes that occur going from one particular shear zone toward the non-metasomatized (pristine) olivine gabbro on Langøy, Norway, was reported by Kusebauch et al. (2015). The modal mineralogy starting at the pristine gabbro consists of olivine, pyroxene, feldspar, and pargasitic amphibole. Heading toward the shear zone, there is a gradual loss of olivine, pyroxene, and plagioclase, an increase in the modal proportion of amphibole, and the appearance of scapolite, biotite, and tourmaline each of which increase in modal abundance until they are all replaced by amphibole at the shear zone. Chlorine is present in amphibole at all distances from the shear zone as shown in Figure 7a. Because there

is a relatively long section where plagioclase (Plag), orthopyroxene (Opx), clinopyroxene (Cpx), and amphibole (Amph) coexist, it is possible to calculate the concentration of $FeCl_2$ and $CaCl_2$ in the metasomatizing fluid at specific locations along the sampling transect using the following reactions:

$$\text{Fe-Cl-Horn}^{\text{Amph}} + \text{CaTs}^{\text{Cpx}} = \text{Hed}^{\text{Cpx}} + 2\ \text{An}^{\text{Plag}} + \text{Fs}^{\text{Opx}} + \text{FeCl}_2{}^{\text{Brine}} \quad (8a)$$

$$\text{Fe-Cl-Horn}^{\text{Amph}} + \text{CaTs}^{\text{Cpx}} = 2\ \text{An}^{\text{Plag}} + 2\ \text{Fs}^{\text{Opx}} + \text{CaCl}_2{}^{\text{Brine}} \quad (8b)$$

where Fs is $Fe_2Si_2O_6$ in orthopyroxene and the remaining abbreviations are the same as those for reaction 5. In reactions 8a,b, $FeCl_2$ and $CaCl_2$ are modeled as the neutral salt dissolved in a brine with the assumption that activity is equal to mole fraction, as was assumed previously for reaction 5. This is undoubtedly a simplistic assumption, but in the absence of more detailed composition-activity data at elevated pressures and temperatures, such as those for NaCl and KCl (Aranovich and Newton, 1997), this assumption will be adopted. The equilibrium constants for reactions 8a and 8b can be rearranged explicitly to solve for the X_{FeCl2} and X_{CaCl2} in the brine as follows:

$$X_{FeCl2}^{Brine} = \frac{K_{8a}^{o}\left(a_{Fe-Cl-Horn}^{Amph}\right)\left(a_{CaTs}^{Cpx}\right)}{\left(a_{Hed}^{Cpx}\right)\left(a_{An}^{Plag}\right)^{2}\left(a_{Fs}^{Opx}\right)} = K_{8a}^{o}K_{8a}' \quad (9a)$$

$$X_{CaCl2}^{Brine} = \frac{K_{8b}^{o}\left(a_{Fe-Cl-Horn}^{Amph}\right)\left(a_{CaTs}^{Cpx}\right)}{\left(a_{An}^{Plag}\right)^{2}\left(a_{Fs}^{Opx}\right)^{2}} = K_{8b}^{o}K_{8b}' \quad (9b)$$

where $K°$ is calculated for the end-member reaction at the P and T of interest as:

$$K^{o} = e^{-\Delta G^{o}/RT} \quad (10)$$

Using the ideal activity expression for the component Fe-Cl-Horn in amphibole given in equation 7 and activities of the other components from the AX62 program (Holland, 2019), mole fractions of $FeCl_2$ and $CaCl_2$ in a presumed coexisting paleobrine were calculated at the sample distances listed in Table 10 all at 2 kbar and 600°C, conditions that were estimated for the

549 scapolitization episode at Langøy (Nijland and Touret, 2001; Engvik et al., 2011). Figure 7b
550 shows the corresponding calculated weight % of $FeCl_2$ and $CaCl_2$ versus distance. Only sample
551 distances for which coexisting mineral compositions were reported (in the Supplementary Tables
552 of Kusebauch et al., 2015), or that could be reasonably well estimated, are given in Table 10 and
553 using the average of multiple analyses when reported.

554 Several things can be seen from this analysis. First, Table 10 shows that the calculated
555 concentrations of $FeCl_2$ and $CaCl_2$ vary in agreement with the Fe-Cl-Horn activities of the
556 amphibole; however, they do not directly follow the total Cl content of the amphibole. Figure
557 7a, based in part on Figure 4 of Kusebauch et al. (2015), shows that the Cl content varies in an
558 asymmetric manner, going from 0.3 wt% Cl in the pristine gabbro (~30 cm from shear zone),
559 reaching a maximum of about 1.1 wt% Cl at a distance of 25.3-21.4 cm, and then gradually
560 decreasing to 0.5 wt% Cl at the shear zone. In contrast, the calculated paleobrine concentrations
561 in Figure 7b reach a maximum at 21.4-18.6 cm. This offset is caused by a slightly higher Fe^{2+}
562 content in the amphiboles at 21.4-18.6 cm giving them a higher Fe-Cl-Horn activity. This
563 illustrates the important point that it is the activity of a given Cl-bearing component in
564 amphibole, rather than the total Cl content, that determines the paleobrine concentration in this
565 type of analysis. Second, the maximum calculated concentrations of 3-4 wt% $FeCl_2$ and 9-10
566 wt% $CaCl_2$ seem low compared to NaCl contents of 24 wt% or more observed in fluid inclusions
567 from nearby metasedimentary rocks (Kusebauch et al., 2015). This may result from several
568 factors, including (i) the current method only calculates the activities of $FeCl_2$ and $CaCl_2$, which
569 may not be the dominant Cl-bearing aqueous species, and (ii) that the ideal-activity expression
570 used here (Equation 7) in a Mg-free system does not adequately model the Fe-Cl-Horn
571 component in Mg-bearing amphiboles or account for the reciprocal mixing of Mg and Fe^{2+} with

572 Cl and OH (e.g., Zhu and Sverjensky, 1992). Extending the activity model presented here to
573 more typical Mg-bearing systems will require additional experimental work involving
574 amphiboles with variable iron and magnesium contents. This will be the subject of a future
575 publication involving potassic-chloro-hastingsite based on the work of Matteucci (2022), where a
576 potentially more accurate method of deriving chloride activities from amphibole phase equilibria
577 will be presented. At the moment, the thermochemical information presented here represents an
578 important first step in determining absolute concentrations of aqueous chloride species, not
579 simply ratios of aqueous species.

580 **Acknowledgments**

581 Thanks are given to David Collins for assisting with the electron microprobe analyses and to
582 Vincent Van Nostrand for assisting with the FTIR analyses. Thanks are given to Mark Kendrick
583 and an anonymous reviewer for their very helpful comments. Financial support for this study
584 comes from NSF grant EAR-1725053 to DMJ, for which the author is grateful.

585

586

587

588 **References Cited**

589 Almeida, K. M. F., and Jenkins, D. M. (2017) Stability field of the Cl-rich scapolite marialite.
590 American Mineralogist, 102, 2484-2493.
591 Aranovich, L. Ya. and Newton, R. C. (1997) H_2O activity in concentrated KCl and KCl-NaCl
592 solutions at high temperatures and pressures measured by the brucite-periclase equilibrium.
593 Contributions to Mineralogy and Petrology, 127, 261-271.

Aranovich, L. and Safonov, O. (2018) Halogens in high-grade metamorphism. In Harlov, D. E. and Aranovich, L. (eds.), The role of halogens in terrestrial and extraterrestrial geochemical processes. Chapter 11, Springer Geochemistry, pp. 713-757.

Barnes, J. D., and Cisneros, M. (2012) Mineralogical control on the chlorine isotope composition of altered oceanic crust. Chemical Geology, 326-327, 52-60.

Bowen, N. L., and Schairer, J. F. (1935) Grünerite from Rockport, Massachusetts, and a series of synthetic fluor-amphiboles. American Mineralogist, 20, 543-551.

Campanaro, B. P., and Jenkins, D. M. (2017) An experimental study of chlorine incorporation in amphibole synthesized along the pargasite—ferro-pargasite join. Canadian Mineralogist, 55, 419-436.

Carpenter, P., Irving, A., and Jolliff, B. (2021) EPMA of amphibole in meteorites: Nakhlite northwest Africa 13368 and Winonaite northwest Africa 13432. Microscopy and Microanalysis, 27 (Supplement S1), 2796-2798, DOI: https://doi.org/10.1017/S143192762100979X.

Chan, A., Jenkins, D. M., and Dyar, M. D. (2016) Partitioning of chlorine between NaCl brines and ferro-pargasite: Implications for the formation of chlorine-rich amphiboles in mafic rocks. Canadian Mineralogist, 54, 337-351.

Cloos, M. (1993) Lithospheric buoyancy and collisional orogenesis: Subduction of oceanic plateaus, continental margins, island arcs, spreading ridges, and seamounts. Geological Society of America Bulletin, 105, 715-737.

Comeforo, J. E., and Kohn, J. A. (1954) Synthetic asbestos investigations, I: Study of synthetic fluor-tremolite. American Mineralogist, 39, 537-548.

Corona, J. C., Jenkins, D. M., and Holland, T. J. B. (2013) Constraints on the upper pressure

stability of blueschist facies metamorphism along the reaction: glaucophane = talc + 2 jadeite in the Na_2O-MgO-Al_2O_3-SiO_2-H_2O system. American Journal of Science, 313, 967-995.

Dale, J., Powell, R., White, R. W., Elmer, F. L., and Holland, T. J. B. (2005) A thermodynamic model for Ca-Na clinoamphiboles in Na_2O-CaO-FeO-MgO-Al_2O_3-SiO_2-H_2O-O for petrological calculations. Journal of Metamorphic Geology, 23, 771-791.

Della Ventura, G., Hawthorne, F. C., and Iezzi, G. (2019) Synthesis and solid solution in "rubidium richterite", $Rb(NaCa)Mg_5Si_8O_{22}(OH,F)_2$. Physics and Chemistry of Minerals, 46, 759-770.

Driesner, T., and Heinrich, C. A. (2007) The system H_2O-NaCl. Part I: Correlation formulae for phase relations in temperature-pressure-composition space from 0 to 1000 °C, 0 to 5000 bar, and 0 to 1 X_{NaCl}. Geochimica et Cosmochimica Acta. 71, 4880-4901.

Enami, M., Liou, J. G., and Bird, D. K. (1992) Cl-bearing amphibole in the Salton Sea geothermal system, California. Canadian Mineralogist, 30, 1077-1092.

Engvik, A. K., Mezger, K., Wortelkamp, S., Bast, R., Corfu, F., Korneliussen, A., Ihlen, P., Bingen, B., and Austrheim, H. (2011) Metasomatism of gabbro – mineral replacement and element mobilization during the Sveconorwegian metamorphic event. Journal of Metamorphic Geology, 29, 399-423.

Fletcher, E. E., and Elsea, A. R. (1964) The effects of high-pressure, high-temperature hydrogen on steel. DMIC Report 202, March 26, 1964, Defense Metals Information Center, Battelle Memorial Institute, Columbus, Ohio, USA, 70 pp.

Frezzotti, M. L., Ferrando, S., Peccerillo, A., Petrelli, M., Tecce, F., and Perucchi, A. (2010) Chlorine-rich metasomatic H_2O-CO_2 fluids in amphibole-bearing peridotites from Injibara

(Lake Tana region, Ethiopian plateau): Nature and evolution of volatiles in the mantle of a region of continental flood basalts. Geochimica et Cosmochimica Acta, 74, 30230-3039.

Frost, B. R. (1991) Introduction to oxygen fugacity and its petrologic importance. Reviews in Mineralogy, 25, 1-9.

Giblin, L. E., Blackburn, W. H., and Jenkins, D. M. (1993) X-ray continuum discrimination technique for the energy dispersive analysis of fine particles. Analytical Chemistry, 65, 3576-3580.

Giesting, P. A., and Filiberto, J. (2016) The formation environment of potassic-chloro-hastingsite in the nakhlites MIL 03346 and pairs and NWA 5790: Insights from terrestrial chloro-amphibole. Meteoritics and Planetary Science, 51, 2127-2153.

Gilbert, M. C. (1966) Synthesis and stability relations of the hornblende ferropargasite. American Journal of Science, 264, 698-742.

Gilbert, M. C., Helz, R. T., Popp, R. K., and Spear, F. S. (1982) Experimental studies of amphibole stability. Reviews in Mineralogy, 9B, 229-353.

Graham, C. M., and Navrotsky, A. (1986) Thermochemistry of the tremolite-edenite amphiboles using fluorine analogues, and applications to amphibole-plagioclase-quartz equilibria. Contributions to Mineralogy and Petrology, 93, 18-32.

Hawthorne, F. C., and Oberti, R. (2007) Amphiboles: Crystal chemistry. Reviews in Mineralogy and Geochemistry, 67, 1-54.

Hawthorne, F. C., and Della Ventura, G. (2007) Short-range order in amphiboles. Reviews in Mineralogy and Geochemistry, 67, 173-222.

660 Hawthorne, F. C., Oberti, R., Harlow, G. E., Maresch, W. V., Martin, R. F., Schumacher, J. C.,
661 and Welch, M. D. (2012) Nomenclature of the amphibole supergroup. American
662 Mineralogist, 97, 2031-2048.
663 Henry, D. J., and Daigle, N. M. (2018) Chlorine incorporation into amphibole and biotite in
664 high-grade iron-formations: Interplay between crystallography and metamorphic fluids.
665 American Mineralogist, 103, 55-68.
666 Holland, T. J. B. (2019) AX62, Activity-composition program for minerals. Website:
667 https://filedn.com/lU1GlyFhv3UuXg5E9dbnWFF/TJBHpages/index.html (accessed August
668 30, 2021).
669 Holland, T. J. B. and Powell, R. (2011) An improved and extended internally consistent
670 thermodynamic dataset for phases of petrological interest, involving a new equation of state
671 for solids. Journal of Metamorphic Geology, 29, 333-383.
672 Holloway, J. R., and Ford, C. E. (1975) Fluid-absent melting of the fluoro-hydroxy amphibole
673 pargasite to 35 kilobars. Earth and Planetary Science Letters, 25, 44-48.
674 Hovis, G., Abraham, T., Hudacek, W., Wildermuth, S., Scott, B., Altomare, C., Medford, A.,
675 Conlon, M., Morris, M., Leaman, A., Almer, C., Tomaino, G., and Harlov, D. (2015)
676 Thermal expansion of F-Cl apatite crystalline solutions. American Mineralogist, 100, 1040-
677 1046.
678 Hughes, J. M., Cameron, M., and Crowley, K. D. (1989) Structural variations in natural F, OH,
679 and Cl apatites. American Mineralogist, 74, 870-876.
680 Iveson, A. A., Webster, J. D., Rowe, M. C., and Neill, O. K. (2017) Major element and halogen
681 (F, Cl) mineral-melt-fluid partitioning in hydrous rhyodacitic melts at shallow crustal
682 conditions. Journal of Petrology, 58, 2465-2492.

683 Jenkins, D. M. (2019) The incorporation of chlorine into calcium amphibole. American
684 Mineralogist, 104, 514-524.
685 Jenkins, D. M., and Corona, J. C. (2006) The role of water in the synthesis of glaucophane.
686 American Mineralogist, 91, 1055-1068.
687 Jenkins, D.M. and Hawthorne, F.C. (1995) Synthesis and Rietveld refinement of amphibole
688 along the join $Ca_2Mg_5Si_8O_{22}F_2$-$NaCa_2Mg_4Ga_3Si_6O_{22}F_2$. Canadian Mineralogist, 33:13-24.
689 Johnson, E. L., Goergen, E. T., Fruchey, B. L. (2004): Right lateral oblique slip movements
690 followed by post-Ottawan (1050-1020 Ma) orogenic collapse along the Carthage-Colton
691 shear zone: Data from the Dana Hill metagabbro body, Adirondack Mountains, New York.
692 In, R. P. Tollo, L. Corriveau, J. McLelland, and M. J. Bartholomew (eds.) Proterozoic
693 tectonic evolution of the Grenville orogeny in North America. Geological Society of
694 America. Memoir, 197, 357-378.
695 Kendrick, M. A., Honda, M., and Vanko, D. A. (2015) Halogens and noble gases in
696 Mathematician Ridge meta-gabbros, NE Pacific: implications for oceanic hydrothermal root
697 zones and global volatile cycles. Contributions to Mineralogy and Petrology, 170, article 43.
698 Kendrick, M. A., Marks, M. A., Godard, M. (2022) Halogens in serpentinised-troctolites from
699 the Atlantis Massif: implications for alteration and global volatile cycling. Contributions to
700 Mineralogy and Petrology, 177(12), Article 110.
701 Kullerud, K. (1996) Chlorine-rich amphiboles: interplay between amphibole composition and an
702 evolving fluid. European Journal of Mineralogy, 8, 355-370.
703 Kusebauch, C., John, T., Barnes, J. D., Klügel, A., and Austrheim, H. O. (2015) Halogen
704 element and stable chlorine isotope fractionation caused by fluid-rock interaction (Bamble
705 Sector, SE Norway). Journal of Petrology, 56(2), 299-324.

706 Locock, A. J. (2014) An Excel spreadsheet to classify chemical analyses of amphiboles
707 following the IMA 2012 recommendations. Computers and Geosciences, 61, 1-22.
708 Marks, N., Schiffman, P., Zierenberg, R. A., Franzson, J., and Fridleifsson, G. Ó. (2010)
709 Hydrothermal alteration in the Reykjanes geothermal system: Insights from Iceland deep
710 drilling program well RN-17. Journal of Volcanology and Geothermal Research. 189, 172-
711 190.
712 Martin, R. F. (2007) Amphiboles in the igneous environment. Reviews in Mineralogy and
713 Geochemistry, 67, 323-358.
714 Martínez, M., Shearer, C. K., and Brearley, A. J. (2023) Ferro-chloro-winchite in Northwest
715 Africa (NWA) 998 apatite-hosted melt inclusion: New insights into the nakhlite parent melt.
716 Geochimica et Cosmochimica Acta, 344, 122-133.
717 Matjuschkin, V., Brooker, R.A., Tattich, B., Blundy, J.D., Stamper, C.C. (2015). Control and
718 monitoring of oxygen fugacity in piston cylinder experiments. Contributions to Mineralogy
719 and Petrology, 169, 9.
720 Matteucci, J. P. (2022) Experimental studies of the crystal structure, pressure-temperature
721 stability, and chlorine partitioning of hastingsitic amphiboles, 156 p. Ph.D. Dissertation,
722 Binghamton University, Binghamton, NY, USA.
723 Matteucci, J. P., Jenkins, D. M., and Dyar, M. D. (2022) The effect of the ^{A}Na-^{A}K ratio on Cl
724 incorporation in hastingsitic amphiboles. Geological Society of America Abstracts with
725 Programs, 54 (5), Abstract 176-5, doi: 10.1130/abs/2022AM-383429.
726 Morrison, J. (1991) Compositional constraints on the incorporation of Cl into amphiboles.
727 American Mineralogist, 76, 1920-1930.

728 Mueller, B. L., Jenkins, D. M., and Dyar, M. D. (2017) Chlorine incorporation in amphiboles
729 synthesized along the magnesio-hastingsite–hastingsite compositional join. European
730 Journal of Mineralogy, 29, 167-180.
731 Nakada, R., Sato, M., Ushioda, M, Tamura, Y., and Yamamoto, S. (2019) Variation of iron
732 species in plagioclase crystals by X-ray absorption fine structure analysis. Geochemistry,
733 Geophysics, Geosystems, 20, 5319-5333.
734 Nijland, T. G., and Touret, J. L. R. (2001) Replacement of graphic pegmatite by graphic albite-
735 actinolite-clinopyroxene intergrowths (Mjåvatn, southern Norway). European Journal of
736 Mineralogy, 13, 41-50.
737 Pavlovich, M. S., Jr., and Jenkins, D. M. (2003) Assessment of cation substitutions along the
738 gallium and fluorine analogue of the tremolite-glaucophane join. American Mineralogist, 88,
739 1486-1495.
740 Popp, R. K. and Bryndzia, L. T. (1992) Statistical analysis of Fe^{3+}, Ti, and OH in kaersutite from
741 alkalic igneous rocks and mafic mantle xenoliths. American Mineralogist, 77, 1250-1257.
742 Price, J. G. (1985) Ideal site mixing in solid solutions, with an application to two-feldspar
743 geothermometry. American Mineralogist, 70, 696-701.
744 Raudsepp, M., Turnock, A. C., and Hawthorne, F. C. (1991) Amphibole synthesis at low
745 pressure: what grows and what doesn't. European Journal of Mineralogy, 3, 983-1004.
746 Robert, J.-L., Della Ventura, G., and Thauvin, J.-L. (1989) The infrared OH-stretching region of
747 synthetic richterites in the system Na_2O-K_2O-CaO-MgO-SiO_2-H_2O-HF. European Journal of
748 Mineralogy, 1, 203-211.

749 Robie, R. A., Hemingway, B. S. (1995) Thermodynamic properties of minerals and related
750 substances at 298.15 K and 1 bar (10^5 Pascals) pressure and at higher temperatures. U.S.
751 Geological Survey Bulletin 2131, Reston, VA, 461 pp.
752 Robinson, P., Spear, F. S., Schumacher, J. C., Laird, J., Klein, C., Evans, B. W., and Doolan, B.
753 L. (1982) Phase relations of metamorphic amphiboles: Natural occurrence and theory.
754 Reviews in Mineralogy and Geochemistry, 9B, 1-227.
755 Sautter, V., Jambon, A., and Boudouma, O. (2006) Cl-amphibole in the nakhlite MIL 03346:
756 Evidence for sediment contamination in a Martian meteorite. Earth and Planetary Science
757 Letters, 252, 45-55.
758 Selverstone, J., and Sharp, Z. D. (2011) Chlorine isotope evidence for multicomponent mantle
759 metasomatism in the Ivrea Zone. Earth and Planetary Science Letters, 310, 429-440.
760 Shaw, H.R., and Wones, D.R. (1964) Fugacity coefficients for hydrogen gas between 0° and
761 1000°C for pressures to 3000 atm. American Journal of Science, 262, 918-929.
762 Sun, J. Yang, Y., Ingrin, J., Wang, Z., and Xia, Q, (2022) Impact of fluorine on the thermal
763 stability of phlogopite. American Mineralogist, 107, 815-825.
764 Toby, B.H. and Von Dreele, R.B. (2013) GSAS-II: The genesis of a modern open-source all
765 purpose crystallography software package. Journal of Applied Crystallography, 46, 544-549.
766 Vanko, D. A. (1986) High-chlorine amphiboles from oceanic rocks: product of highly-saline
767 hydrothermal fluids? American Mineralogist, 71, 51-59.
768 Weidner, J. R. (1989) Welding silver and silver alloy containers for high-temperature and high-
769 pressure experiments. American Mineralogist, 74, 1385.

770 Welch, M. D., and Pawley, A. R. (1991) Tremolite: New enthalpy and entropy data from a
771 phase equilibrium study of the tremolite = 2 diopside + 1.5 orthoenstatite + β-quartz + H_2O.
772 American Mineralogist, 76, 1931-1939.
773 Yardley, B. W. D., and Bodnar, R. J. (2014) Fluids in the continental crust. Geochemical
774 Perspectives, 3, 1-123.
775 Zhu, C. and Sverjenksy, D. A. (1992) F-Cl-OH partitioning between biotite and apatite.
776 Geochimica et Cosmochimica Acta, 56, 3435-3467.
777

778 Table 1. Starting material synthesis conditions and products.

Sample Code	*T* (°C)	*P* (kb)	*t* (hrs)	$\log(f_{H2})$[a]	$\Delta\log(f_{O2})$[b]	Products and comments
Ferro-chloro-pargasite bulk composition						
FEPG 1-10	949(3)	2.10(5)	144	1.84(1)	-0.02(3)	plag, cpx, fay, halite, $FeCl_2 \cdot nH_2O$, glass(?); capsule is $Ag_{70}Pd_{30}$
FEPG 1-11	600(5)	2.04(5)	365	[1.4(1)]	[-0.2(1)]	amph, plag, halite, $FeCl_2 \cdot nH_2O$
FEPG 1-14	600(5)	2.02(5)	357	[1.4(1)]	[-0.2(1)]	amph, plag, fay, halite, $FeCl_2 \cdot nH_2O$
Ferro-pargasite bulk composition						
FEPG 3-24	800(18)	2.35(5)	93	1.86(1)	-0.27(5)	amph, plag, cpx, gt
FEPG 3-26	952(24)	1.7(2)	17	1.49(6)	+0.52(4)	plag, cpx, mt, sp

779 Note: Uncertainties in the last digit are given in parentheses. Products are listed in decreasing
780 abundance as estimated from the powder XRD patterns. Abbreviations: amph = amphibole, cpx
781 = hedenbergitic clinopyroxene, fay = fayalite, gt = garnet, mt = magnetite, plag = plagioclase,
782 qtz = quartz, sp = hercynitic spinel.
783 [a]Hydrogen fugacities (fH_2), indicated as $\log(fH_2)$, are those imposed by a H_2-Ar mixture as
784 described in the text; values in brackets were calculated from the estimated fO_2.
785 [b]Oxygen fugacity (fO_2) indicated as $\log(fO_2)$ relative to that of the Co-CoO oxygen buffer of Frost
786 (1991). Values in square brackets are estimated for the cold-seal vessels used for these two
787 experiments, as discussed in Jenkins (2019).
788
789
790

This is the peer-reviewed, final accepted version for American Mineralogist, published by the Mineralogical Society of America.
The published version is subject to change. Cite as Authors (Year) Title. American Mineralogist, in press.
DOI: https://doi.org/10.2138/am-2023-8981. http://www.minsocam.org/

Table 2. Electron microprobe analyses of phases synthesized in this study at the conditions indicated in Table 1 and used as starting materials. Cations were calculated on the basis of 6 and 8 oxygens for pyroxene and plagioclase, respectively, and 24 O+OH+Cl for amphiboles. Iron in the pyroxene is assumed to be all Fe^{2+}, while the ferric-iron fraction in plagioclase is assumed to be 0.70 and for amphibole is assumed to be 0.18, as discussed in the text.

Oxide/atom	Sample code and phase							
	FEPG 1-10	FEPG 1-10	FEPG 3-26	FEPG 3-26		FEPG 1-11	FEPG 1-14	FEPG 3-24
wt%	cpx	plag	cpx	plag	wt%	amph	amph	amph
n	12	10	12	12	*n*	15	18	14
SiO_2	45.2(12)	46.2(20)	45.6(10)	55.4(15)	SiO_2	41.3(12)	39.2(27)	36.2(27)
Al_2O_3	1.98(6)	32.7(10)	4.2(5)	26.5(12)	Al_2O_3	8.5(10)	9.3(13)	15.8(24)
FeO[a]	37.8(43)	1.64(75)	26.6(5)	1.34(62)	FeO[a]	34.5(10)	32.9(22)	27.2(31)
CaO	13.5(36)	17.1(5)	21.3(5)	9.95(4)	CaO	9.52(90)	9.46(78)	9.77(94)
Na_2O	0.06(5)	1.39(39)	0.53(10)	3.56(19)	Na_2O	1.46(22)	1.65(17)	3.33(43)
Total	98.6(9)	99.0(14)	98.3(15)	99.1(27)	Cl	1.78(26)	1.59(17)	0.01(1)
cations					Total	97.1(19)	94.1(48)	92.3(64)
Si	1.94(3)	2.15(7)	1.90(2)	2.52(3)	Total–Cl=O	96.7(19)	93.8(48)	92.3(64)
^{IV}Al	0.06(3)	1.79(6)	0.10(2)	1.42(5)	atoms			
$^{IV}Fe^{3+}$	----	0.04(2)	----	0.04(2)	Si	6.75(15)	6.60(19)	6.07(20)
Sum T	2.00	3.99(2)	2.00	3.98(1)	Al-Tet	1.25(15)	1.40(19)	1.93(20)

^{VI}Al	0.04(2)	----	0.10(1)	----	Sum T	8.00	8.00	8.00
Fe^{2+}	1.36(16)	0.02(1)	0.93(1)	0.02(1)	Al-C	0.39(8)	0.45(12)	1.18(38)
Ca	0.62(16)	0.85(3)	0.95(1)	0.49(2)	Fe^{3+}-C	0.85(3)	0.84(4)	0.69(7)
Na	0.00	0.12(3)	0.04(1)	0.52(3)	Fe^{2+}-C	3.76(6)	3.71(9)	3.13(32)
Total cations	4.02(2)	4.99(2)	4.02(2)	5.00(1)	Sum C	5.00	5.00	5.00
An (Plag)	----	0.86(3)	----	0.48(2)	Fe-B	0.11(11)	0.09(10)	0.00
					Ca-B	1.67(14)	1.71(11)	1.75(9)
					Na-B	0.22(5)	0.20(6)	0.25(10)
					Sum B	2.00	2.00	2.00
					Na-A	0.24(9)	0.34(8)	0.84(10)
					Ca-A	0.00	0.00	0.00
					Total cations	15.24(9)	15.34(8)	15.84(10)
					Cl	0.49(7)	0.45(4)	0.00
					OH[b]	1.51(7)	1.51(4)	1.47(47)

Values reported are the average of *n* analyses, and uncertainties (1σ) in the last digit given in parentheses.
[a] Total Fe reported as FeO
[b] Estimated by adding sufficient OH to either have the sum of OH+Cl in the W sites equal 2.0, or the sum of T- and C-site cations (excluding Ca, Na, and K) equal 13.

This is the peer-reviewed, final accepted version for American Mineralogist, published by the Mineralogical Society of America.
The published version is subject to change. Cite as Authors (Year) Title. American Mineralogist, in press.
DOI: https://doi.org/10.2138/am-2023-8981. http://www.minsocam.org/

800

801 Table 3. Reversal mixtures used in this study

Reversal mixture code prefix	Starting material (from Table 1)				
	FEPG 1-10 (no amph)	FEPG 1-11 (amph)	FEPG 1-14 (amph)	FEPG 3-24 (amph)	FEPG 3-26 (no amph)
Ferro-chloro-pargasite bulk composition ($NaCa_2(Fe_4Al)(Al_2Si_6)O_{22}Cl_2$)					
CLFP 1	X	X	----	----	----
CLFP 2	X	----	X	----	----
Ferro-pargasite bulk composition ($NaCa_2(Fe_4Al)(Al_2Si_6)O_{22}(OH)_2$)					
FEPG 7	----	----	----	X	X
FEPG 8	----	----	----	X	X

802 Note: X indicates starting material was used in the reversal mixture; ---- indicates it was not
803 used.

804

805

806 Table 4. Reaction reversal experimental conditions and results.

Sample Code	*T* (°C)	*P* (kb)	*t* (hrs)	log(fH_2)[a]	Δlog(fO_2)[b]	Products and comments
Ferro-chloro-pargasite bulk composition – lower fO_2						
CLFP 2-1	461(3)	1.08(5)	335	0.91(3)	-0.35(7)	amph growth, with plag, fay, halite, cpx present
CLFP 2-2	540(5)	0.93(5)	351	1.07(3)	-0.26(5)	amph growth, with plag, fay, cpx, halite, $FeCl_2 \cdot nH_2O$ present
CLFP 2-3	580(3)	0.93(5)	166	1.17(2)	-0.26(4)	weak amph growth, with plag, fay, halite, cpx, $FeCl_2 \cdot nH_2O$ present
CLFP 2-4	620(3)	0.98(5)	335	1.29(2)	-0.29(3)	amph breakdown, with plag, fay, cpx, halite, $FeCl_2 \cdot nH_2O$ present
CLFP 1-8	562(3)	2.18(5)	303	1.38(3)	-0.29(4)	amph growth, with plag, halite, fay present, no cpx
CLFP 1-7	600(5)	1.75(6)	120	1.38(2)	-0.22(4)	no reaction; amph, plag, fay, hed, halite present
CLFP 1-6	640(4)	2.05(6)	193	1.56(1)	-0.30(3)	amph breakdown with plag, fay, cpx, halite present
Ferro-chloro-pargasite bulk composition – higher fO_2						
CLFP 2-11	589(3)	1.00(5)	165	0.84(5)	0.49(9)	amph growth, with plag, fay, halite, cpx(?) present
CLFP 2-10	610(7)	0.96(5)	184	0.86(5)	0.52(9)	amph breakdown, with plag, fay, cpx, halite, $FeCl_2 \cdot nH_2O$ present
CLFP 2-14	630(4)	1.02(5)	144	0.93(3)	0.50(7)	no reaction; amph, plag, fay, cpx, halite, $FeCl_2 \cdot nH_2O$ present
CLFP 2-15	640(3)	0.95(5)	260	0.92(3)	0.52(7)	amph breakdown, with plag, fay, cpx, halite, $FeCl_2 \cdot nH_2O$ present
CLFP 2-6	557(3)	2.05(5)	243	0.98(5)	0.46(9)	amph growth, with plag, fay, cpx, halite, $FeCl_2 \cdot nH_2O$ present
CLFP 2-7	630(4)	2.09(5)	172	1.16(5)	0.47(10)	amph growth, with plag, fay, cpx, halite, $FeCl_2 \cdot nH_2O$ present
CLFP 2-9	649(5)	2.10(5)	170	1.21(3)	0.46(7)	no reaction; amph, plag, fay halite present
CLFP 2-8	670(3)	2.08(5)	261	1.23(3)	0.49(7)	amph breakdown, with plag, fay, cpx, halite, $FeCl_2 \cdot nH_2O$ present
CLFP 2-13	670(3)	3.00(10)	142	1.36(4)	0.49(7)	amph growth, with plag, cpx, fay, halite, $FeCl_2 \cdot nH_2O$ present
CLFP 2-12	710(4)	2.98(12)	140	1.43(3)	0.50(6)	amph breakdown, with plag, cpx, fay, halite, $FeCl_2 \cdot nH_2O$ present
Ferro-pargasite bulk composition						
FEPG 8-1	560(4)	0.46(5)	212	0.55(4)	0.55(8)	no reaction; amph, plag, cpx, mt, gt present

FEPG 8-2	578(4)	0.45(5)	221	0.60(4)	0.52(9)	no reaction; amph, plag, cpx, mt, gt present
FEPG 8-3	600(4)	0.49(5)	213	0.67(4)	0.51(8)	slight amph breakdown, with plag, cpx, mt, gt present
FEPG 7-12	550(3)	1.12(5)	303	0.80(4)	0.43(8)	amph growth, with plag, cpx, mt, gt present
FEPG 7-14	575(4)	1.07(6)	240	0.84(3)	0.46(7)	amph growth, with plag, cpx, mt, gt present
FEPG 7-11	601(3)	1.00(5)	217	0.86(2)	0.51(6)	no reaction; amph, plag, cpx, mt, gt present
FEPG 7-15	615(3)	0.98(5)	190	0.88(3)	0.50(5)	slight breakdown of amph, with plag, cpx, mt, gt present
FEPG 7-13	630(5)	0.96(5)	192	0.91(3)	0.51(6)	amph breakdown, with plag, cpx, mt, gt, sp present
FEPG 7-10	691(9)	1.10(5)	236	1.10(2)	0.42(3)	strong amph breakdown, with plag, cpx, mt, gt present
FEPG 7-9	780(3)	1.00(5)	165	1.18(2)	0.46(4)	no amph; plag, cpx, mt, gt present
FEPG 7-8	780(4)	2.10(5)	216	1.42(2)	0.48(3)	amph growth, with plag, cpx, mt present
FEPG 7-2	796(6)	2.15(5)	135	1.46(2)	0.47(4)	amph growth, with plag, cpx present, no mt
FEPG 7-1-1	810(2)	2.15(5)	192	1.48(2)	0.47(4)	no amph; plag, cpx, mt present
FEPG 7-7	810(4)	1.98(5)	222	1.43(1)	0.50(3)	no amph; plag, cpx, gt, sp, mt present
FEPG 7-6	820(10)	2.15(5)	192	1.49(1)	0.47(3)	no reaction, with amph, plag, cpx present, no mt
FEPG 7-5	840(7)	2.11(5)	239	1.50(1)	0.48(3)	amph breakdown, with plag, cpx present
FEPG 7-4	860(9)	2.18(5)	136	1.54(1)	0.47(3)	amph breakdown, with plag, cpx, mt, gt present
FEPG 7-3	880(5)	2.15(5)	120	1.55(1)	0.48(3)	amph breakdown, with plag, cpx, mt present

Note: Uncertainties in the last digit are given in parentheses. Abbreviations as in Table 1.

[a] The fH_2, reported as the log(fH_2), is that imposed on the system by the H_2-Ar pressure medium of the internally-heated gas vessel, as discussed in the text.

[b] The fO_2 is expressed as the log(fO_2) relative to the Co-CoO oxygen buffer and is calculated from the imposed fH_2 as discussed in the text.

814
815 Table 5. Electron microprobe analyses of amphiboles from selected reaction-reversal
816 experiments at the conditions indicated in Table 4.

Oxide (wt%)	CLFP 2-11	CLFP 2-7	CLFP 2-13	FEPG 7-12	FEPG 7-8	CLFP 1-6
n	12	13	12	12	11	10
SiO_2	41.5(15)	40.1(17)	41.0(10)	33.2(38)	37.0(7)	40.3(32)
Al_2O_3	9.4(11)	10.0(8)	9.80(92)	14.6(19)	14.7(6)	8.5(11)
FeO[a]	34.6(12)	32.9(14)	33.8(10)	26.6(20)	30.9(3)	34.0(21)
CaO	10.2(7)	9.98(53)	9.90(69)	9.6(13)	10.9(2)	9.51(37)
Na_2O	1.82(21)	1.98(16)	2.09(22)	3.23(38)	3.57(13)	1.84(18)
Cl	1.61(21)	1.61(16)	1.63(18)	0.0	0.01(1)	1.74(17)
Total	99.1(17)	96.6(30)	98.2(19)	87.2(87)	97.2(14)	95.0(49)
Total-Cl=O	98.7(17)	96.3(30)	97.8(19)	----	----	95.6(49)
atoms						
Si	6.65(13)	6.57(10)	6.62(10)	5.93(18)	6.00(5)	6.68(20)
Al-T	1.35(13)	1.43(10)	1.38(10)	2.07(18)	2.00(5)	1.32(20)
Sum T	8.00	8.00	8.00	8.00	8.00	8.00
Al-C	0.42(12)	0.51(12)	0.48(9)	1.00(18)	0.81(7)	0.35(10)
Fe^{3+}-C	0.84(4)	0.81(3)	0.82(2)	0.72(3)	0.75(1)	0.85(2)
Fe^{2+}-C	3.75(9)	3.68(9)	3.70(7)	3.28(15)	3.44(6)	3.80(8)
Sum C	5.00	5.00	5.00	5.00	5.00	5.00
Fe-B	0.06(8)	0.03(5)	0.05(6)	0.00	0.00	0.07(4)
Ca-B	1.74(12)	1.75(9)	1.71(11)	1.82(10)	1.89(4)	1.69(8)
Na-B	0.20(8)	0.22(7)	0.24(6)	0.18(10)	0.11(4)	0.24(8)

Sum B	2.00	2.00	2.00	2.00	2.00	2.00
Ca-A	0.00	0.00	0.00	0.01(3)	0.00	0.00
Na-A	0.37(12)	0.41(8)	0.41(10)	0.94(5)	1.01(3)	0.36(12)
Total cations	15.37(12)	15.41(8)	15.41(10)	15.95(5)	16.01(3)	15.36(12)
Cl	0.44(6)	0.45(4)	0.45(5)	0.00	0.00	0.49(7)
OH[b]	1.49(16)	1.46(15)	1.47(16)	1.57(34)	1.53(9)	1.51(7)

Values reported are the average of *n* analyses, and uncertainties (1σ) in the last digit given in parentheses.

[a] Total Fe reported as FeO

[b] Estimated by adding sufficient OH to either have the sum of OH+Cl in the W sites equal 2.0, or the sum of T- and C-site cations (excluding Ca, Na, and K) equal 13.

Table 6. Electron microprobe analyses of clinopyroxene from selected reaction-reversal experiments at the conditions indicated in Table 4. Cations calculated on the basis of 6 oxygens with all iron assumed to be Fe^{2+}.

Oxides (wt%)	CLFP 2-15	CLFP 2-8	CLFP 2-12	FEPG 7-13	FEPG 7-7
n	11	11	11	7	8
SiO_2	47.7(12)	46.6(14)	47.9(7)	45.0(8)	45.6(11)
Al_2O_3	2.4(15)	2.15(86)	1.90(82)	4.9(11)	4.48(35)
FeO[a]	30.4(15)	34.1(18)	31.8(21)	27.4(5)	28.0(7)
CaO	18.9(10)	16.7(14)	18.7(14)	21.3(2)	21.3(5)
Na_2O	0.28(21)	0.16(18)	0.21(17)	0.43(7)	0.52(11)
Total	99.7(12)	99.8(14)	100.5(10)	99.1(7)	99.9(17)
atoms					
Si	1.96(4)	1.95(4)	1.97(2)	1.86(3)	1.88(2)
^{IV}Al	0.04(4)	0.06(3)	0.03(2)	0.14(3)	0.22(2)
Sum T	2.00	2.00(1)	2.00	2.00	2.00
^{VI}Al	0.08(4)	0.05(2)	0.06(2)	0.10(2)	0.09(1)
Fe^{2+}	1.05(6)	1.19(7)	1.09(7)	0.95(2)	0.96(2)
Ca	0.83(4)	0.75(5)	0.82(6)	0.94(1)	0.94(1)
Na	0.02(2)	0.01(1)	0.02(1)	0.04(1)	0.04(1)
Total cations	3.99(2)	4.01(2)	3.99(1)	4.03(1)	4.04(1)
a_{Hed} [b]	0.82	0.85	0.83	0.82	0.80
a_{CaTs} [b]	0.18	0.12	0.13	0.17	0.12

Values reported are the average of *n* analyses, and uncertainties (1σ) in the last digit are given in parentheses.

[a] Total Fe reported as FeO; [b]Activities calculated at the *P* and *T* of treatment (Table 4).

833 Table 7. Electron microprobe analyses of plagioclase from selected reaction-reversal
834 experiments at the conditions indicated in Table 3. Cations calculated on the basis of 8 oxygens
835 with the fraction of ferric iron fixed at 0.7 (see text).

Oxide (wt%)	CLFP 2-15	CLFP 2-8	CLFP 2-12	FEPG 7-13	FEPG 7-7
n	10	12	12	6	12
SiO_2	46.9(17)	47.2(21)	46.6(26)	55.1(28)	54.6(16)
Al_2O_3	32.4(16)	33.4(19)	33.5(41)	26.3(14)	27.4(14)
FeO[a]	1.5(12)	1.06(29)	1.52(98)	1.15(46)	0.41(19)
CaO	16.3(9)	16.7(18)	16.0(12)	10.1(11)	10.6(14)
Na_2O	2.02(26)	1.89(92)	1.98(50)	5.71(65)	5.33(72)
Total	99.2(29)	100.2(15)	99.6(31)	98.3(46)	98.4(18)
atoms					
Si	2.18(2)	2.16(9)	2.16(12)	2.53(4)	2.50(7)
Al	1.77(4)	1.81(10)	1.80(14)	1.42(4)	1.48(6)
Fe^{3+}	0.04(4)	0.03(1)	0.04(3)	0.03(1)	0.011(5)
Sum Tet.	3.99(1)	4.00(1)	4.00(1)	3.98(1)	3.99(1)
Fe^{2+}	0.02(2)	0.012(3)	0.02(1)	0.01(1)	0.005(2)
Ca	0.81(2)	0.82(9)	0.79(5)	0.50(5)	0.52(7)
Na	0.18(2)	0.17(8)	0.18(5)	0.51(5)	0.47(6)
Total	5.00(1)	5.00(1)	5.00(2)	5.00(1)	4.99(1)
a_{Ab}	0.39	0.36	0.36	0.59	0.53
a_{An}	0.85	0.86	0.85	0.73	0.69

836 Values reported are the average of *n* analyses, and uncertainties (1σ) in the last digit given in
837 parentheses.
838 [a] Total Fe reported as FeO; [b]Activities calculated at the *P* and *T* of treatment (Table 4).
839

Table 8. Thermochemical data adopted in this study for end-member ferro-chloro-hornblende used, along with data for the other phases from Holland and Powell (2011), to calculate *G'* for reaction (5) in the text.

Parameter		Value
$V_{298K,\ 1bar}$ (cm^3/mol)		283.0
C_P* (kJ/K·mol)	*a*	1.106
	b	8.9156 x 10^{-5}
	c	-11,218.3
	d	-5.9548
α (K^{-1})**		2.88 x 10^{-5}
κ (kbar)		760.00
κ '		4.10
κ " (kbar^{-1})		-0.0054

* The heat capacity terms (*a*, *b*, *c*, and *d*) are the coefficients in the expression $C_P = a + b(T) + c/(T^2) + d/(T^{0.5})$, where *T* is in Kelvins and have units that give the heat capacity (C_P) in kJ/K·mol.

** Values of α, κ, κ ', and κ " for ferro-chloro-hornblende are those of ferro-actinolite from Holland and Powell (2011).

Note: $G' = \int_{T_0}^{T} \Delta C_P^{reaction}\, dT - T \int_{T_0}^{T} \frac{\Delta C_P^{reaction}}{T} dT + \int_{P_0}^{P} \Delta V^{solids} dP + RT ln K_a$

This is the peer-reviewed, final accepted version for American Mineralogist, published by the Mineralogical Society of America.
The published version is subject to change. Cite as Authors (Year) Title. American Mineralogist, in press.
DOI: https://doi.org/10.2138/am-2023-8981. http://www.minsocam.org/

Table 9. Values of enthalpy of formation (ΔH_f°) and third-law entropies (S°) at 298 K and 1 bar based on the experimental data of Cl-OH-amphibole stability for a given mole fraction (X_{FeCl2} = activity) of $FeCl_2$ and corresponding K_a value for reaction (5) in the text.

X_{FeCl2}	K_a	ΔH_f° 298K, 1bar (kJ/mol)	S° 298K, 1bar (J/K·mol)
0.1	39.1	-10,842.6 ± 10.3	627.6 ± 11.1
0.3	117.4	-10,842.6 ± 10.3	618.6 ± 11.1
0.5	195.7	-10,842.6 ± 10.3	614.2 ± 11.1

This is the peer-reviewed, final accepted version for American Mineralogist, published by the Mineralogical Society of America.
The published version is subject to change. Cite as Authors (Year) Title. American Mineralogist, in press.
DOI: https://doi.org/10.2138/am-2023-8981. http://www.minsocam.org/

853

854 Table 10. Component activities and calculated mole fractions and equivalent weight % (wt%) of $FeCl_2$ and $CaCl_2$ at metasomatic
855 conditions of 600 °C and 2 kbar for a paleobrine coexisting with the Langøy, Norway, metagabbros reported by Kusebauch et al.
856 (2015).

Sample Distance	$a_{FeClHorn}^{Amph}$	a_{An}^{Plag}	a_{Fs}^{Opx}	a_{Hed}^{Cpx}	a_{CaTs}^{Cpx}	K'_{8a}	K'_{8b}	X_{FeCl2}	wt% $FeCl_2$	X_{CaCl2}	wt% $CaCl_2$
30 cm (PG)	0.000013(2)	0.76	0.063	0.19	0.074	0.00014(2)	0.00042(6)	0.00009(1)	0.06(1)	0.00025(4)	0.15(2)
25.9	9.77E-06	0.79	0.052	0.17	0.077	0.00014	0.00045	0.000090	0.06	0.00027	0.16
23.6	0.00016(9)	0.76	0.064	0.17	0.039	0.0010(6)	0.0026(15)	0.0007(3)	0.5(3)	0.0016(9)	0.96(53)
21.4	0.00041(4)	0.76	*0.064*	0.30	0.178	0.0066(6)	0.031(3)	0.0043(4)	3.0(3)	0.018(2)	10.4(9)
18.6	0.00076(24)	0.75	*0.064*	0.19	0.086	0.0096(30)	0.028(9)	0.0064(20)	4.3(13)	0.017(5)	9.6(27)
14.7	0.00009(5)	0.76	0.064	*0.19*	*0.086*	0.0011(6)	0.0033(19)	0.0007(4)	0.5(3)	0.0019(11)	1.2(6)

857 Note: Samples are indicated by their distance (cm) from the shear zone in the Langøy, Norway, site studied by Kusebauch et al.
858 (2015) with PG indicating the pristine gabbro. Entries in italics were estimated from neighboring samples. Uncertainties in the last
859 digit (given in parentheses) are based only on the variations in the activities of the Fe-Cl-Horn component in amphibole arising from
860 the standard deviation (1σ) in the averages of the amphibole analyses at a given distance, if multiple analyses were reported. Values
861 for K^o are K_{8a}^o = 0.6627 and K_{8b}^o = 0.5975.

862

Figure Captions

Figure 1. Representative back-scattered electron (BSE) images of the starting materials synthesized in this study. (A) Amphibole-rich starting material made from ferro-chloro-pargasite bulk composition (FEPG 1-11, Table 1). (B) Amphibole breakdown starting material made from ferro-chloro-pargasite bulk composition (FEPG 1-10, Table 1). (C) Amphibole-rich starting material made from (hydroxy-) ferro-pargasite bulk composition (FEPG 3-24, Table 1). (D) Amphibole breakdown starting material made from ferro-pargasite bulk composition (FEPG 3-26, Table 1). Abbreviations as in Table 1. Scale bar in all images is 10 μm.

Figure 2. Comparison of the upper-thermal stability of Cl-bearing amphiboles investigated in this study (Table 4) at two different oxygen fugacities imposed by different H_2-Ar atmospheres. Results at 0.3 log(fO_2) below Co-CoO showing growth (solid triangles), no reaction (grey triangles), or breakdown (open triangles) of amphibole. Dashed boundary is fitted by eye to these lower fO_2 results. Results at 0.5 log(fO_2) above Co-CoO showing growth (solid circles), no reaction (grey circles), and breakdown (open circles) of amphibole. Solid boundary is a linear regression to the bracketing data.

Figure 3. Upper-thermal stability of ferro-pargasite determined in this study at 0.5 log(fO_2) above Co-CoO, which is ≈ 0.2 log(fO_2) below the fayalite-magnetite-quartz (FMQ) buffer, compared with the upper-thermal stability curve reported by Gilbert (1966) determined at the FMQ oxygen buffer.

Figure 4. (a) Upper-thermal stability of the Cl-OH-amphibole compared with (b) the upper-thermal stability of ferro-pargasite.

Figure 5. FTIR spectra of the synthetic amphiboles used as starting materials in this study (Table 2). Vertical dashed lines indicate absorption bands associated with structural OH vibrations in amphibole, while the double-headed arrow indicates broad OH vibrations associated with surface water absorbed by the sample.

Figure 6. Representative G' vs T plot for reaction (5) in the text, for $X_{FeCl2} = 0.3$. Short line segments connect experimental points bracketing the location of an isopleth between the growth (solid squares) and breakdown (open squares) of amphibole at a given pressure. Long line is a linear regression to the mid-points of each experimental bracket.

Figure 7. (a) Chlorine content of amphiboles (wt%) in metagabbros vs distance from the shear zone (SZ) to the pristine gabbro (PG) at Langøy, Norway, reported by Kusebauch et al. (2015). Vertical dashed lines indicate changes in mineral assemblage. (b) Calculated weight % of $FeCl_2$ (solid squares) and $CaCl_2$ (open squares) of paleobrines based on reactions 8a and 8b in the text, as listed in Table 10.

902

903 Figure 1

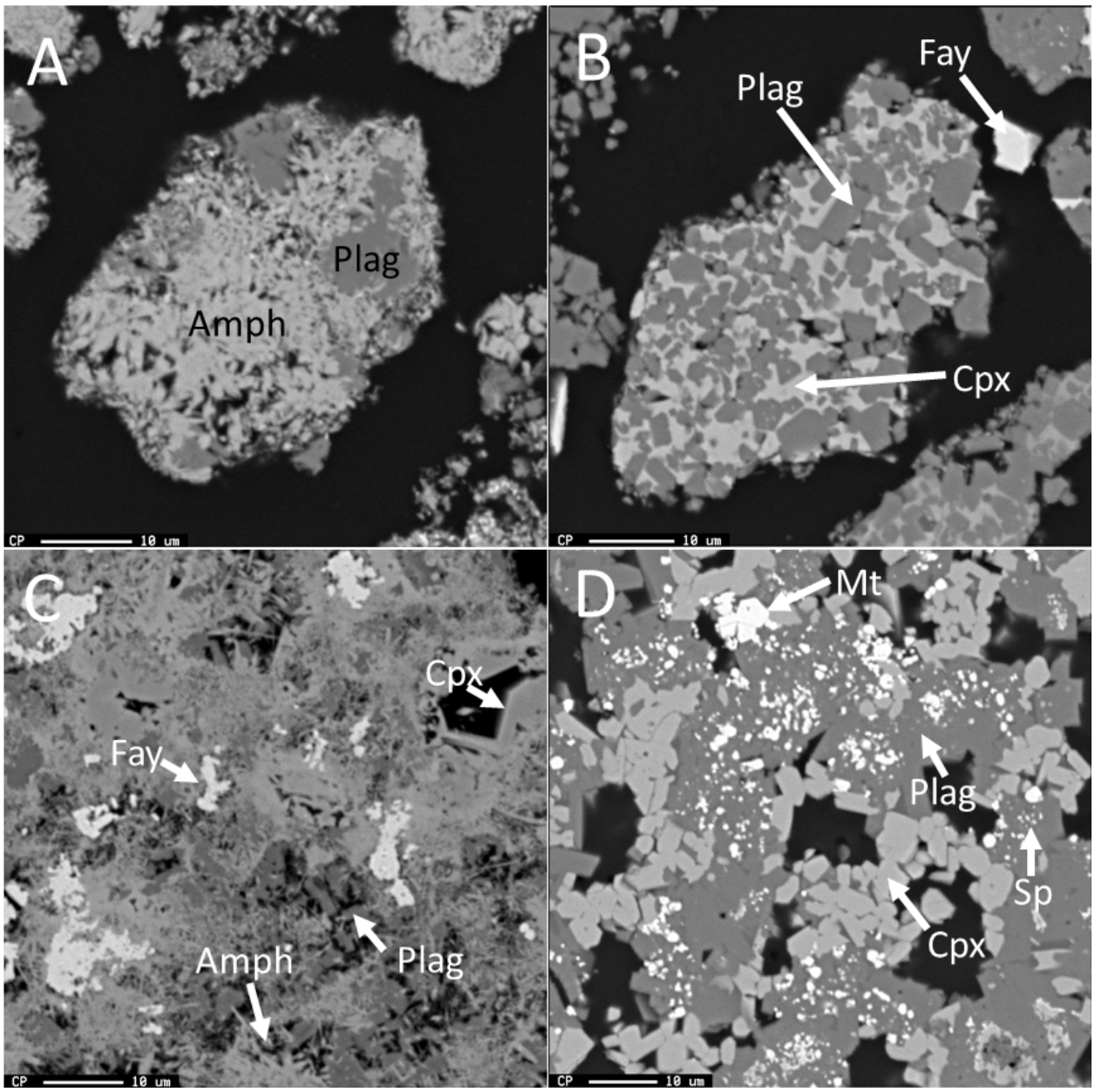

904

905

This is the peer-reviewed, final accepted version for American Mineralogist, published by the Mineralogical Society of America.
The published version is subject to change. Cite as Authors (Year) Title. American Mineralogist, in press.
DOI: https://doi.org/10.2138/am-2023-8981. http://www.minsocam.org/

906 Figure 2

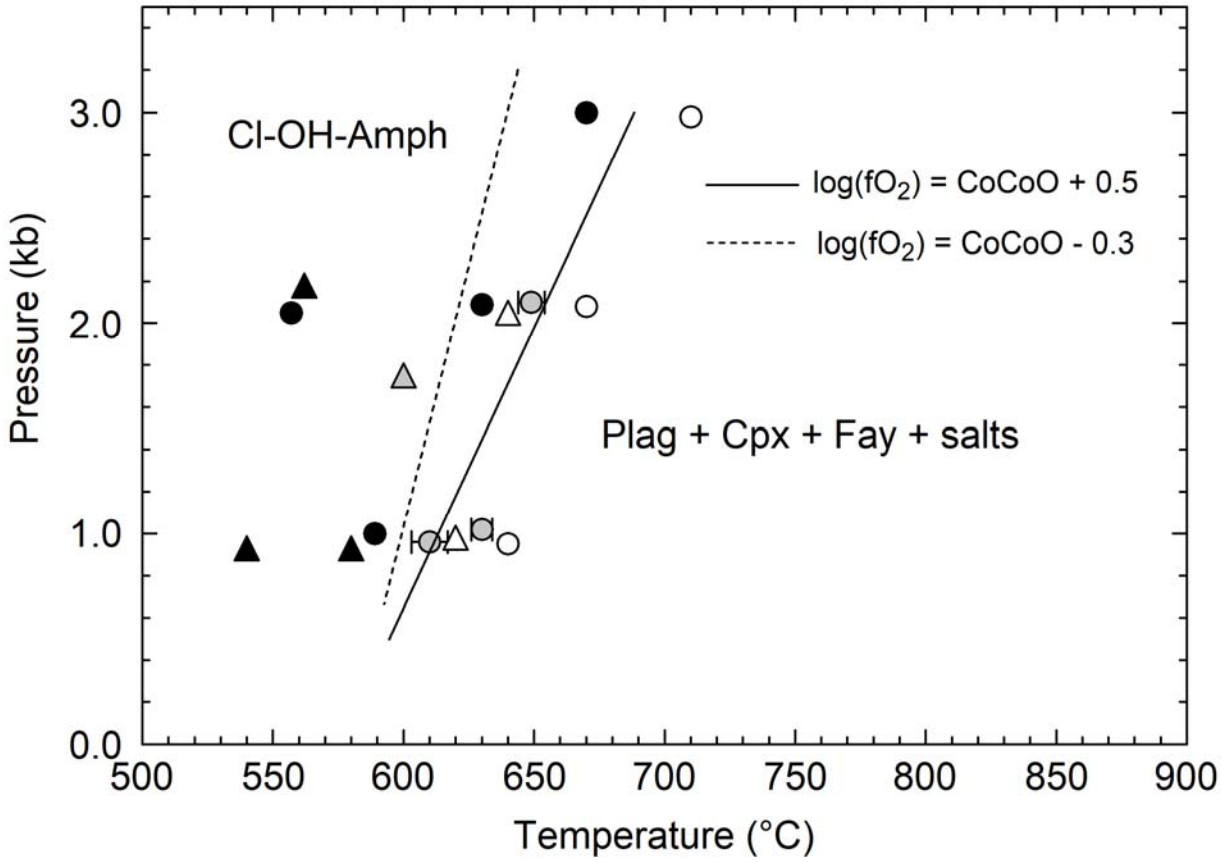

907

908

This is the peer-reviewed, final accepted version for American Mineralogist, published by the Mineralogical Society of America.
The published version is subject to change. Cite as Authors (Year) Title. American Mineralogist, in press.
DOI: https://doi.org/10.2138/am-2023-8981. http://www.minsocam.org/

909 Figure 3

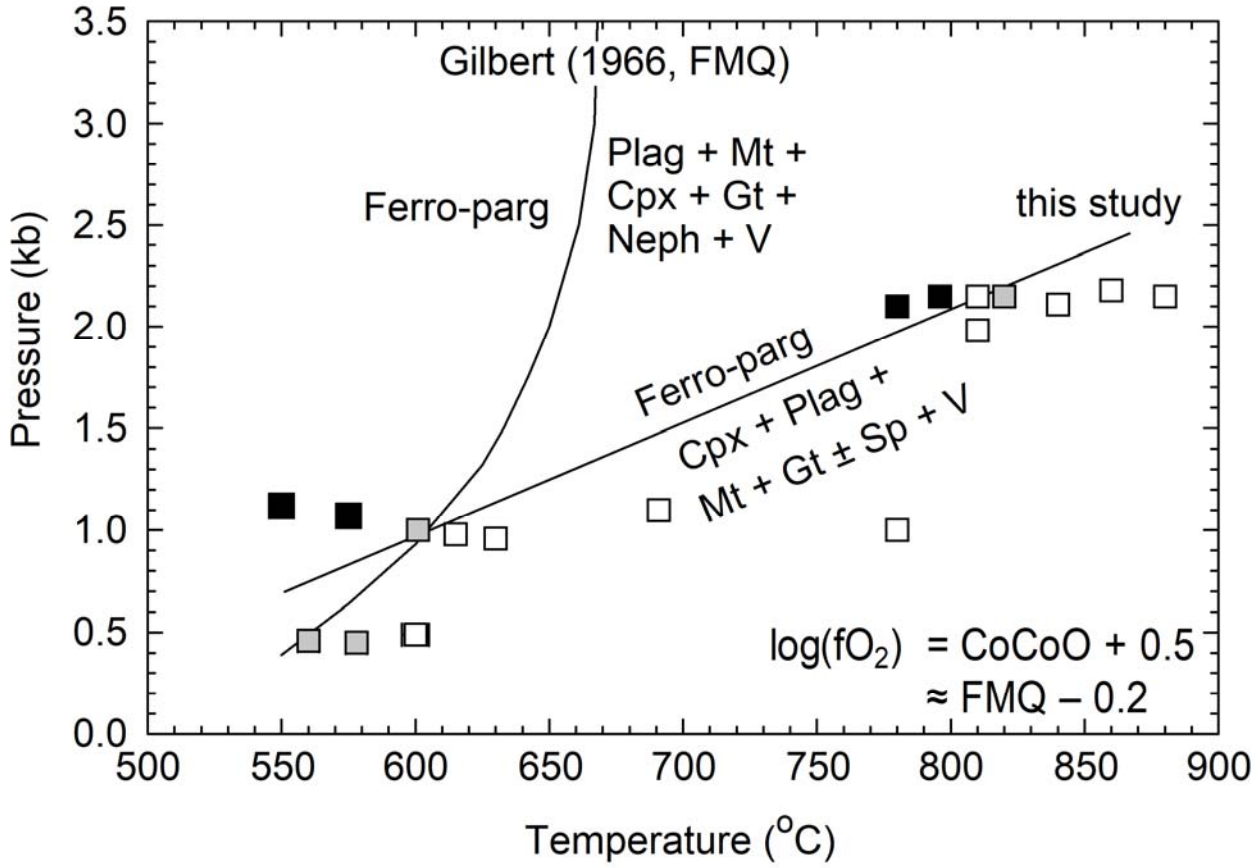

910

911

912

913

This is the peer-reviewed, final accepted version for American Mineralogist, published by the Mineralogical Society of America.
The published version is subject to change. Cite as Authors (Year) Title. American Mineralogist, in press.
DOI: https://doi.org/10.2138/am-2023-8981. http://www.minsocam.org/

914 Figure 4

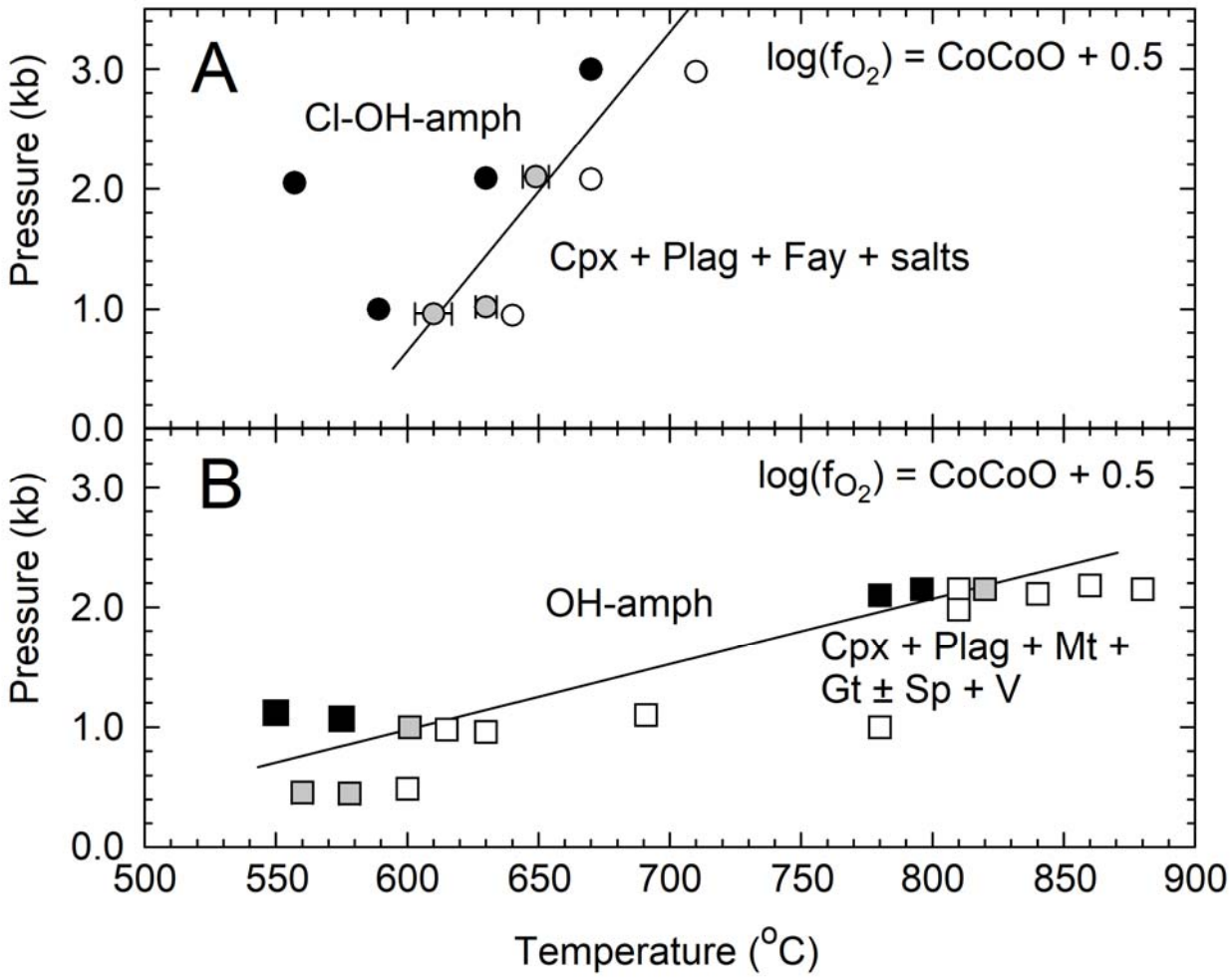

915

916

917 Figure 5

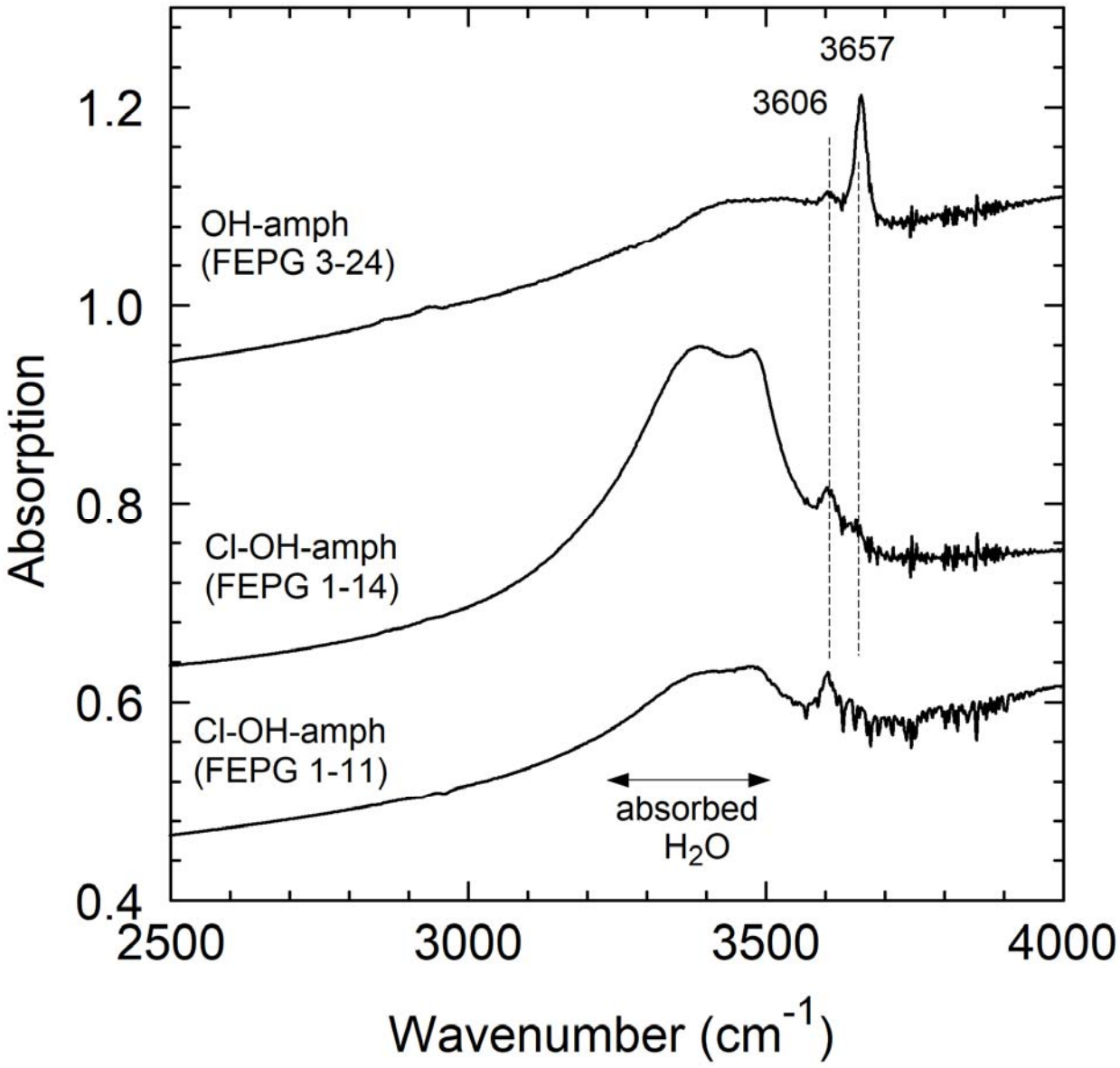

918

919

920

This is the peer-reviewed, final accepted version for American Mineralogist, published by the Mineralogical Society of America.
The published version is subject to change. Cite as Authors (Year) Title. American Mineralogist, in press.
DOI: https://doi.org/10.2138/am-2023-8981. http://www.minsocam.org/

921 Figure 6

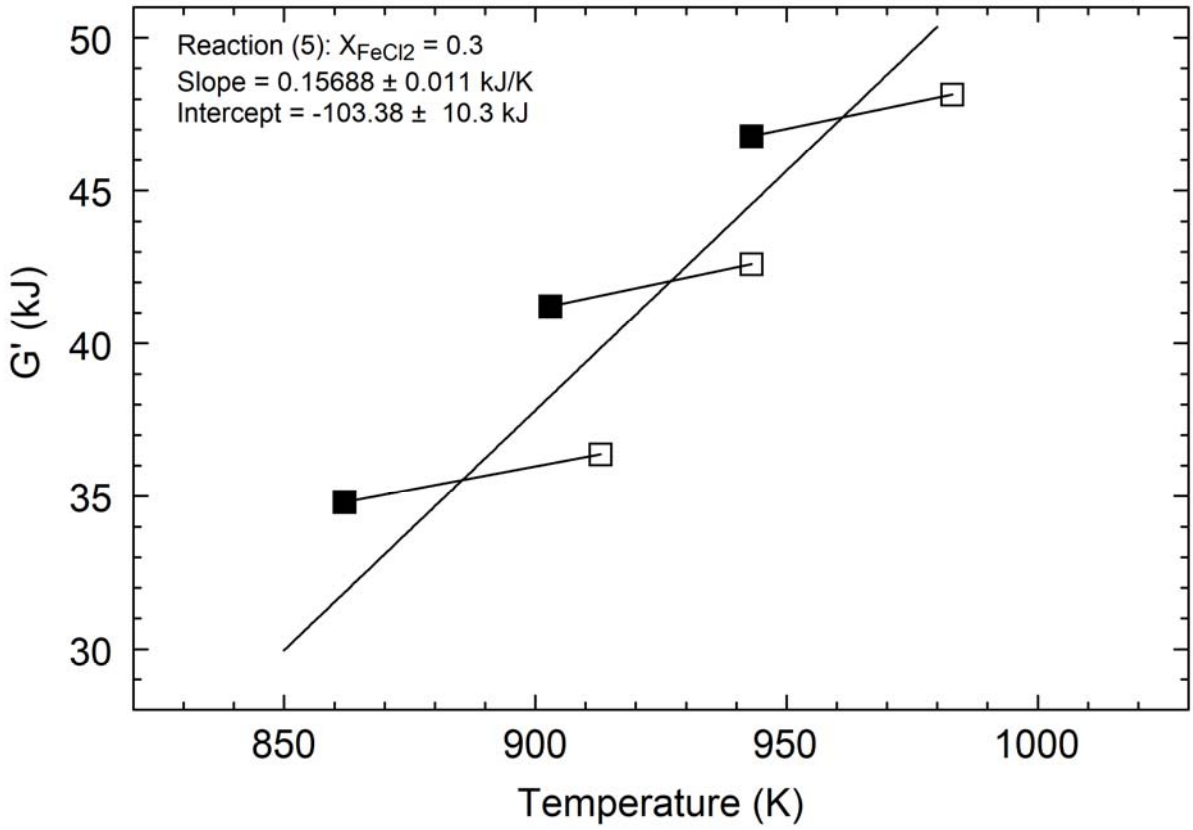

922

923

924 Figure 7

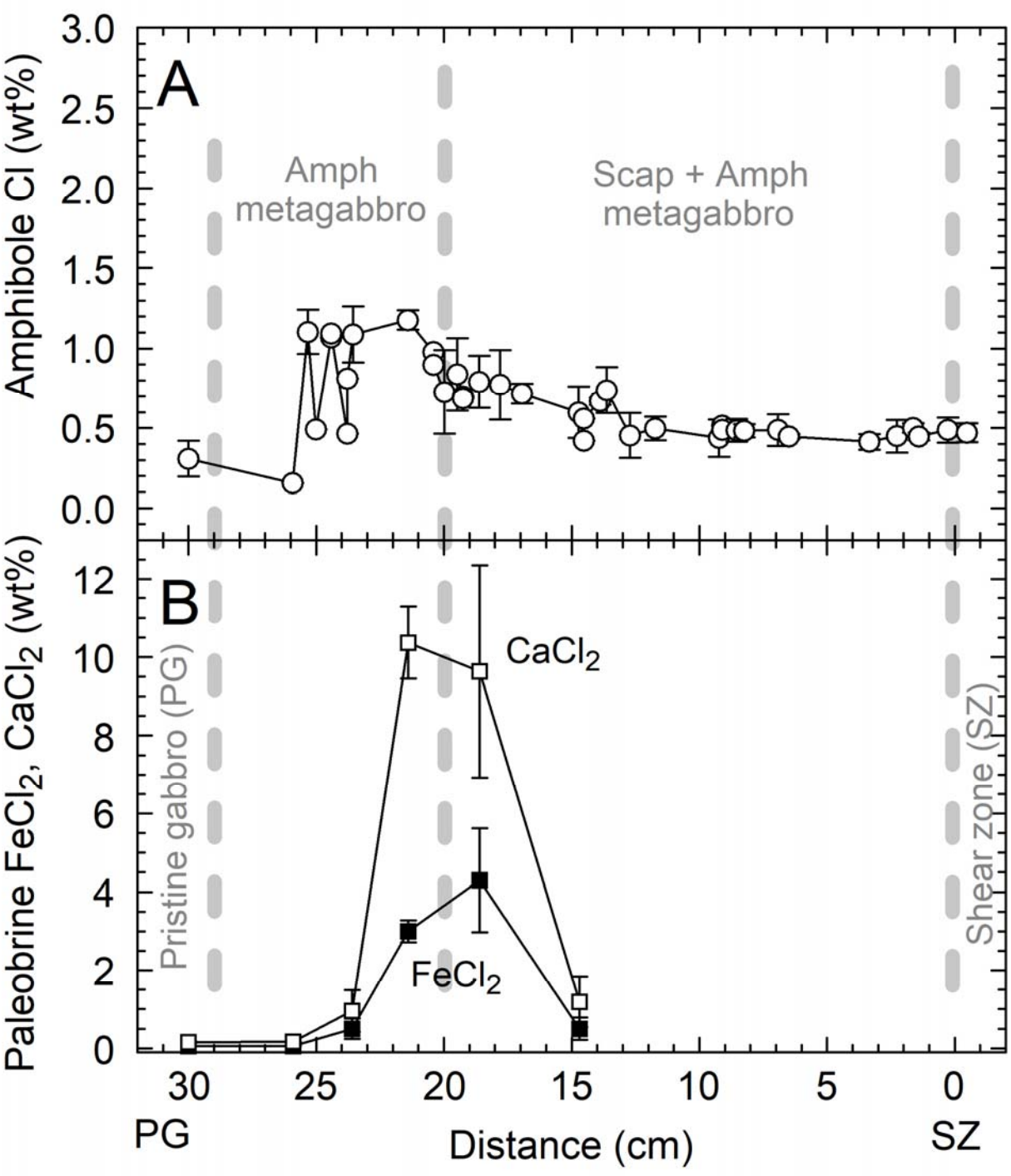

925

926